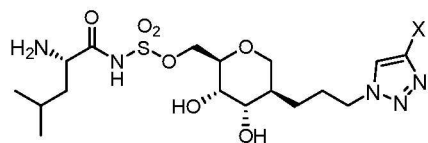


This item is the archived peer-reviewed author-version of:

Synthesis and structure-activity studies of novel anhydrohexitol-based Leucyl-tRNA synthetase inhibitors

Reference:

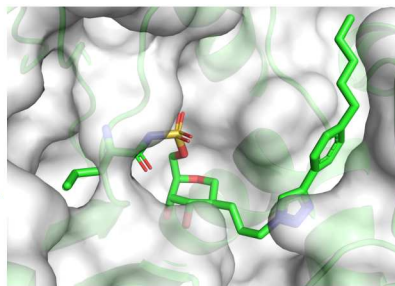
De Ruyscher Dries, Pang Luping, Lenders Stijn M.G., Cappoen Davie, Cos Paul, Rozenski Jef, Strelkov Sergei V., Weeks Stephen D., Van Aerschot Arthur.-
Synthesis and structure-activity studies of novel anhydrohexitol-based Leucyl-tRNA synthetase inhibitors
European journal of medicinal chemistry - ISSN 0223-5234 - 211(2021), 113021
Full text (Publisher's DOI): <https://doi.org/10.1016/J.EJMECH.2020.113021>
To cite this reference: <https://hdl.handle.net/10067/1747840151162165141>



11 novel LeuRS inhibitors;

11a: X = 4-pentylphenyl

$K_i^{\text{app}} = 5.5 \text{ nM}$



11a bound in the active site of LeuRS

Journal Pre-proof

Synthesis and Structure-Activity Studies of Novel Anhydrohexitol-based Leucyl-tRNA Synthetase Inhibitors

Dries De Ruyscher^{a,#}, Luping Pang^{a,b,#}, Stijn M.G. Lenders^a, Davie Cappoen^c, Paul Cos^c, Jef Rozenski^a, Sergei V. Strelkov^b, Stephen D. Weeks^{b,d,*},¹ and Arthur Van Aerschot^{a,*},¹

^a Medicinal Chemistry, Rega Institute for Medical Research, Department of Pharmaceutical and Pharmacological Sciences, KU Leuven, Herestraat 49 – Box 1030, 3000 Leuven, Belgium

^b Biocrystallography, Department of Pharmaceutical and Pharmacological Sciences, KU Leuven, Herestraat 49 – Box 822, 3000 Leuven, Belgium

^c Laboratory of Microbiology, Parasitology and Hygiene, Department of Pharmaceutical Sciences, University of Antwerp, Universiteitsplein 1, 2610 Wilrijk, Belgium

^d Present address: *OrthogonX, Gaston Geenslaan 1, 3001 Leuven, Belgium*

* Corresponding author.

E-mail address: arthur.vanaerschot@kuleuven.be (A. Van Aerschot);

sweeks@orthogontherapeutics.com (S.D. Weeks).

These authors contributed equally to this work.

¹ Both authors equally supervised and gave guidance to this work.

Abstract

Leucyl-tRNA synthetase (LeuRS) is a clinically validated target for the development of antimicrobials. This enzyme catalyzes the formation of charged tRNA^{Leu} molecules, an essential substrate for protein translation. In the first step of catalysis LeuRS activates leucine using ATP, forming a leucyl-adenylate intermediate. Bi-substrate inhibitors that mimic this chemically labile phosphoanhydride-linked nucleoside have proven to be potent inhibitors of different members of the aminoacyl tRNA synthetase family but, too date, they have demonstrated poor antibacterial activity. We synthesized a small series of 1,5-anhydrohexitol based analogues coupled to a variety of triazoles and performed detailed structure-activity relationship studies with bacterial LeuRS. In an *in vitro* assay, K_i^{app} values in the nanomolar range were demonstrated. Inhibitory activity differences between the compounds revealed that the polarity and size of the triazole substituents affect binding. X-ray crystallographic studies of *N. gonorrhoeae* LeuRS in complex with all the inhibitors highlighted the crucial interactions defining their relative enzyme inhibitory activities. We further examined their *in vitro* antimicrobial properties by screening against several bacterial and yeast strains. While only weak antibacterial activity against *M. tuberculosis* was detected, the extensive structural data which were obtained could make these LeuRS inhibitors a suitable starting point towards further antibiotic development.

Keywords

Leucyl-tRNA synthetase – bisubstrate competitive inhibitors – protein-ligand co-crystal structures – structure-activity relationship – enzyme inhibition

1. Introduction

The World Health Organization (WHO) stated in a recent report that by 2050 10 million people would die every year as a result of the rapid expansion of antimicrobial resistance [1]. Hence, as part of a global action plan, this agency has highlighted the importance of investment in the development of new treatments [2]. One strategy to identify new antibiotic classes is to explore novel or underexplored cellular targets. Aminoacyl-tRNA synthetases (aaRSs) are a family of enzymes, which play a pivotal role in protein biosynthesis in all cells. Due to the wide evolutionary divergence of aminoacyl-tRNA synthetases (aaRSs) in pathogenic organisms with respect to the human orthologues, these enzymes are promising targets for the development of new selective antimicrobials [3,4]. Although various aaRSs have been targeted for drug design, only the IleRS inhibitor mupirocin [5] (Figure 1A) and the LeuRS targeting compound AN2690 (tavaborole [6], Figure 1A) have made it to the clinic, used for the treatment of methicillin-resistant *Staphylococcus aureus* (MRSA) and onychomycosis, a fungal infection of the toenails, respectively.

The aminoacylation reaction of LeuRS proceeds in two steps [3]. Both steps occur within the same catalytic site defined by a class I specific Rossmann fold containing the HIGH and KMSKS signature motifs [7]. Besides its cognate substrate, LeuRS is also able to activate structurally similar amino acids including isoleucine (Ile), methionine (Met), norvaline and norleucine with a frequency exceeding the tolerable translational error by the cell [8-10]. Therefore, this enzyme has evolved a proofreading function which can either hydrolyze the misactivated amino acid in the active site by pre-transfer editing, or clear mischarged tRNA through post-transfer editing [11]. The latter is catalysed by an additional editing domain which is inserted into the Rossmann fold *via* two β -strands [12]. For bacterial LeuRS, the post-transfer editing is the dominant error-correction pathway.

The validated LeuRS inhibitor AN2690 targets the editing domain by forming a stable boron-mediated tRNA^{Leu}-AN2690 adduct. It traps the 3'-end of the tRNA^{Leu} isoacceptor in a non-productive state which prevents subsequent LeuRS catalytic turnover and consequently, disrupts protein synthesis [6]. Generally, benzoxaborole-containing compounds display low toxicity and high specificity [13] and importantly, tavaborole demonstrated no resistance after repeated exposure [14]. However, the development of the antibacterial 3-aminomethyl analogue GSK2251052 (AN3365, Figure 1A), which could evade the main efflux mechanism of multidrug-resistant (MDR) Gram-negative bacteria [15], was terminated after evaluation in phase II clinical trials owing to the rapid development of resistance [16]. This was a result of the appearance of cells carrying editing domain mutations that were highly resistant to the compound without compromised viability. A similar appearance of IleRS mutants is also the cause for the low- and high-level resistance in the case of mupirocin [17-20]. More recently, another boron-containing molecule GSK3036656 (Figure 1A) was synthesized and preclinically evaluated as a selective inhibitor against the editing domain of *Mycobacterium tuberculosis* (*Mtb*) LeuRS rather than human cytoplasmic and mitochondrial orthologues. This compound demonstrated *in vitro* activity against the *Mtb* strain H37Rv with a MIC value of 23.5 ng/mL and an IC₅₀ value of 58.8 ng/mL against *Mtb* LeuRS in an aminoacylation assay [21]. It emerged as a promising lead candidate and was selected for further clinical development.

As the editing domain is highly degenerate or fully lost in a number of LeuRSs from *Mycoplasma* parasites [22], the canonical aminoacylation site in the catalytic domain is still popular for targeted drug design. The majority efforts to target this site have concentrated on identifying non-hydrolysable analogues of the natural aminoacyl-adenylate (aa-AMP) intermediate [15]. Compounds like leucyl-sulfamate adenosine (LeuSA, Figure 1B) demonstrate high affinity but exhibit poor selectivity and low *in vivo* antibacterial activity. As a consequence, in the late 1990s, research shifted towards other scaffolds. Cubist Pharmaceuticals (since 2015 acquired by Merck & Co.) used the high-affinity ligand LeuSA as a starting point to synthesize inhibitors with improved chemical stability and bacterial selectivity [23]. The adenine group was replaced by substituted thiazoles which were directly attached to the ribose ring [24]. However, despite their high affinity and selectivity towards bacterial LeuRS, no antibacterial activity was reported. A similar approach gave rise to selective IleRS inhibitors in which the sugar ring was connected with aryl-substituted tetrazoles *via* a two-carbon atom linker (Figure 1B) [25]. The (phenoxyphenyl)tetrazole CB 432 was reported to possess good

antibacterial activity, but low *in vivo* bioavailability halted further exploration of this scaffold for potential antibiotics. More recently, scientists at Oxford Drug Design have reported LeuRS inhibitors that target the enzyme active site [26]. Synthesis of these gram-negative bacteria-selective *N*-leucanyl benzenesulfonamides was based on previously reported benzenesulfonamide ThrRS inhibitors [27]. Similar *N*-leucanyl benzenesulfonamides further connected to an acylated thiourea scaffold were synthesized which appeared to exhibit good inhibitory activity against *Trypanosoma brucei* LeuRS [28, 29].

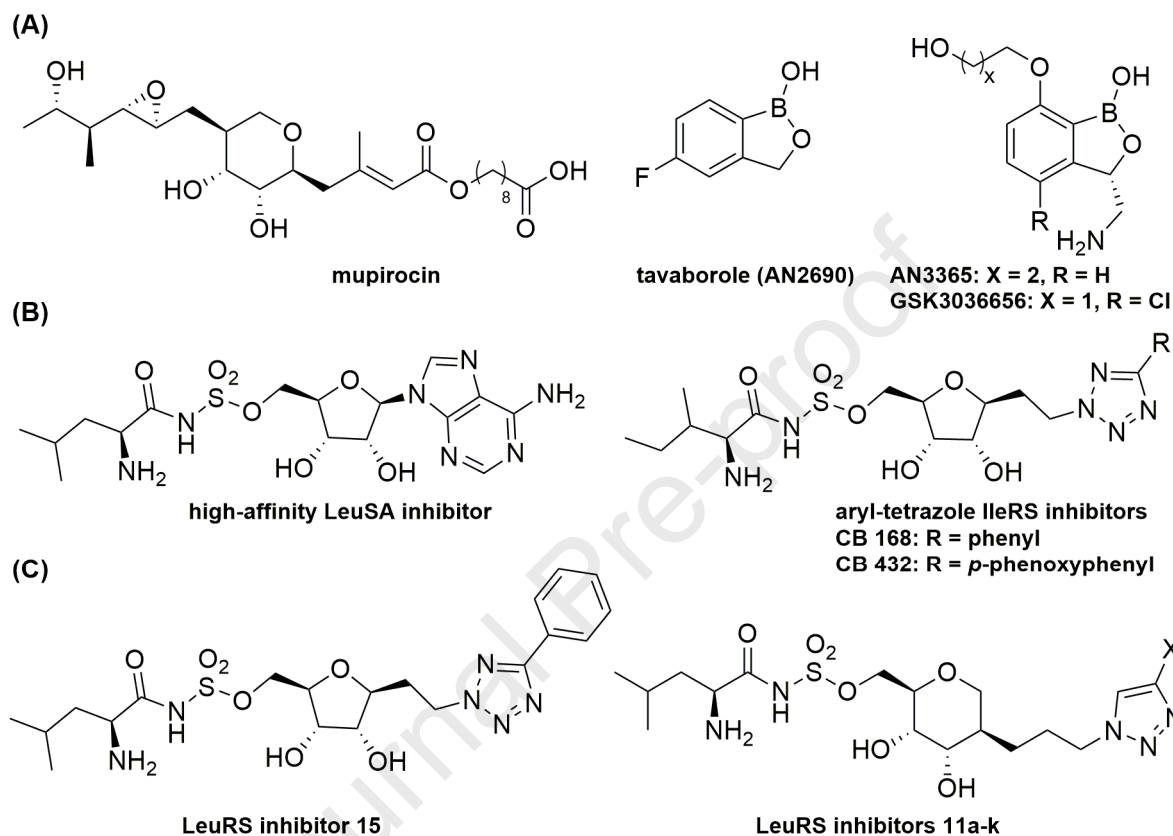
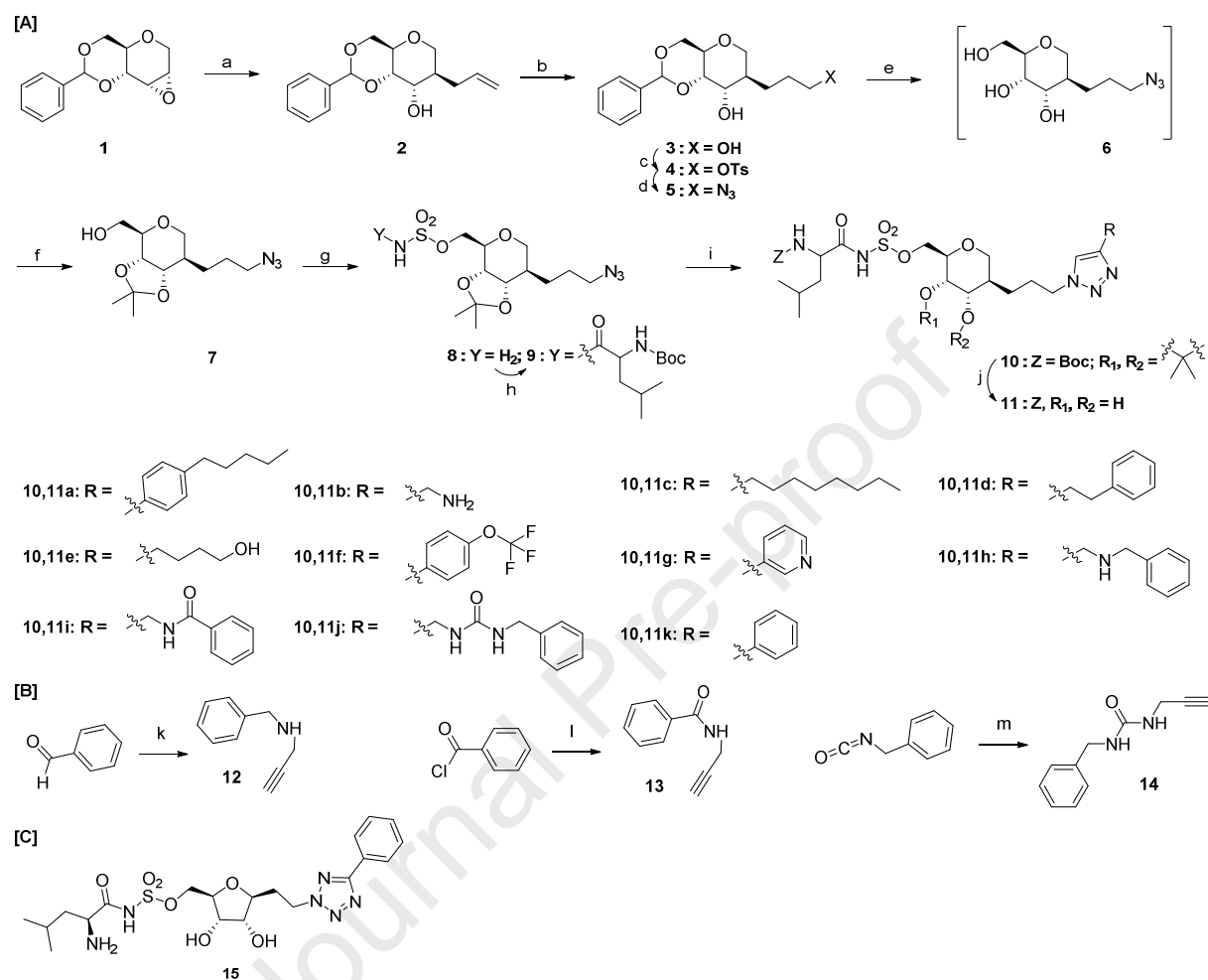


Figure 1. (A) Structures of mupirocin, tavorole, AN3365 and GSK3036656; (B) (Left) High-affinity but non-selective competitive active site inhibitor LeuSA, (Right) Cubist Pharmaceuticals aryl-tetrazole IleRS inhibitors; (C) (Left) Cubist Pharmaceuticals derived LeuRS inhibitor, (Right) Structure for the novel proposed competitive inhibitors targeting LeuRS.

We recently published the synthesis of IleRS inhibitors having good affinity [30] where we substituted the ribose ring of CB 168 (Figure 1B) with a 1,5-anhydrohexitol ring with implantation of the aliphatic chain at C2 and the isoleucyl-sulfamoyl chain at C5, respectively. The three-atom linker between phenyltriazole and the pyran ring was proven to be essential for preserving good affinity for IleRS. Unfortunately, no antibacterial activity was observed, probably resulting from the high polarity of the IleRS inhibitors. We therefore envisioned synthesis of LeuRS inhibitors with the same scaffold and implantation of both side chains on the ring, but with various substituted triazoles to improve antibacterial activity (Figure 1C). Following synthesis of compounds **11a-k**, their inhibition activity and antibacterial activity were evaluated. Combined with high-resolution crystal structures of the enzyme-ligand complexes, we were able to carry out a small but thorough SAR study to provide better insight into the crucial interactions for the substituted triazole to obtain potent enzymatic inhibitory activity.

2. Results

2.1. Synthesis of LeuRS inhibitors containing different substituted triazoles



Reagents and conditions: [A] (a) (1) CuI, allyl-MgCl, anh. THF, -30 °C, 15 min.; (2) **1**, anh. THF, -30 °C, 1.5 h; (b) BH₃·THF, anh. THF, rt, 1 h; (2) NaOH, H₂O₂, H₂O, 0 °C to rt, overnight; (c) (1) TEA, anh. DCM, 0 °C; (2) TsCl, anh. DCM, 0 °C to rt, 2 d; (d) NaN₃, anh. DMF, 55 °C, overnight; (e) PTSA·H₂O, THF:H₂O, 40 °C, 3 d; (f) PTSA·H₂O, DMP, acetone, rt, overnight; (g) (1) chlorosulfonyl isocyanate, HCOOH, 0 °C, 30 min.; (2) anh. MeCN, rt, 5 h; (3) **7**, DMA, rt, overnight; (h) Boc-Leu-OSu, Cs₂CO₃, anh. DMF, 0 °C to rt, 3 d; (i) CuI, TEA, respective alkyne, DMF, 50 °C, overnight; (j) TFA:H₂O, rt, 5 h; [B] (k) (1) propargylamine, acetic acid, anh. MeOH, rt, overnight; (2) NaBH₄, 0 °C to rt, 2 h; (l) TEA, propargylamine, anh. DCM, 0 °C to rt, overnight; (m) propargylamine, anh. DCM, 0 °C to rt, 3 h.

Scheme 1. [A] Procedure towards various leucine coupled triazoles **11**; [B] Synthesis of non-commercially available alkynes; [C] Cubist Pharmaceuticals-like inhibitor **15**.

The envisaged target compounds **11a-k** were based on the potent tetrazole IleRS inhibitors of Cubist Pharmaceuticals (Figure 1B) [25]. The reported enzymatic activity of the latter ranged from 0.5 to 20 nM depending on the pathogen sources, and these compounds were endowed with high selectivity for bacterial IleRS versus the human orthologue. LeuRS shares high structural similarity with IleRS and both belong to the same aaRS Ia subclass. In addition, the inhibitory activity of LeuSA ($K_i^{\text{app}} = 0.14$ nM) is substantially higher than the equivalent isoleucine coupled analogue for IleRS

($K_i^{\text{app}} = 1.92 \text{ nM}$) [31]. This improved affinity for LeuRS targeting compounds was also noted with base modified inhibitors compared to those for IleRS [32], which further stimulated our choice for LeuRS as the target for the synthesis of compounds **11a-k**. These novel inhibitors are based on the CB 168 Cubist Pharmaceuticals compound (Figure 1B), but in which the ribose ring is replaced by a pyran ring so that the implantation of both side chains is moved by one carbon atom. We previously reported that for this particular chain arrangement, the optimal aliphatic linker between the six-membered ring and the heterocycle is a C3 spacer [30].

The synthetic route commenced with commercially available allitol epoxide **1** (Scheme 1). The Gilman-reagent of allylmagnesium chloride was made to open the epoxide regio- and stereoselectively at the C2-position in a trans-diaxial manner [33]. The obtained alkene **2** underwent a hydroboration-oxidation reaction, followed by selective tosylation of the resulting primary alcohol, which afforded compound **5** upon subsequent *in situ* azide substitution allowing the coupling of a series of alkynes. Hereto, the azide **5** was converted into the isopropylidene protected alcohol **7**. Subsequent sulfamoylation was followed by coupling leucine to the obtained sulfamate functional group, affording compound **9**. At this stage, we connected 11 different alkynes using conventional azide-alkyne click chemistry, affording the protected compounds **10**. The alkyne **12** as needed for **10h** was made through reductive amination, while alkynes **13** and **14** (respectively for synthesis of **10i** and **10j**) were synthesized using standard chemistry. Finally, acidic removal of all protecting groups yielded the desired compounds **11a-k**. The Cubist Pharmaceuticals-like inhibitor **15** (Scheme 1C) was prepared for comparative reasons, and its synthesis is analogous to the original isoleucine analogue [34].

2.2. In vitro enzymatic inhibitory activity

The ability of all new leucine coupled compounds **11a-k** and **15** to inhibit LeuRS was verified using a previously described *in vitro* aminoacylation assay, monitoring the effect on the transfer of the ^{14}C -radiolabeled leucine to tRNA^{Leu} (Table 1 and Supplementary figure 1) [35]. Purified recombinant *E. coli* LeuRS was employed with a total tRNA pool from the same pathogen. We herein opted for *E. coli* LeuRS to carry out the enzymatic assay as many inhibitors before have been tested on this specific enzyme, which allows to compare these different inhibitors for future studies.

Compared with the high-affinity non-hydrolysable Leu-AMP analogue LeuSA (K_i^{app} of 0.14 nM), all novel synthesized compounds demonstrated decreased inhibitory activity, but most of them were still potent binders with K_i^{app} values in the lower nanomolar range. Despite compounds **11a-k** sharing a similar chemical scaffold, different substitutions connected with the triazole moiety showed significant effects on the inhibitory potential. As shown in Table 1, the best compounds **11a** and **11k** carried a phenyl substituent at C13 on the triazole ring (for carbon numbering, see structure in Table 1), showing K_i^{app} values of 5.51 and 2.48 nM, respectively, whereas compound **11f** with an additional para-OCF₃ modification on the phenyl ring or compound **11g** substituting the phenyl with a 3-pyridinyl moiety, showed 3 to 10-fold reduced activity. It suggested that the phenyl substituent is a crucial element in determining the stronger LeuRS inhibition, while any electron-withdrawing modification at this position displayed an opposite trend.

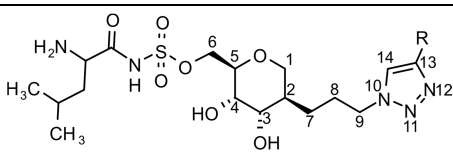
An attempt was made to investigate the effect of a spacer between the triazole and phenyl rings. Consequently, each two to five-atom linker evaluated (compounds **11d** and **11i-j**) led to a significant decrease in binding affinity. Furthermore, compounds **11c** and **11e**, carrying only an aliphatic chain on the triazole moiety, likewise showed reduced inhibitory activity. In addition, it should be noted that both compounds **11b** and **11h** carrying an amine which is protonated physiologically, completely lost their inhibitory activity. Overall, we demonstrated that only 4-phenyltriazole modified compounds are endowed with favorable inhibitory potential.

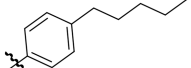
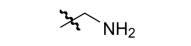
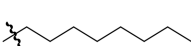
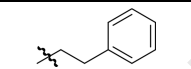
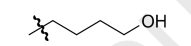
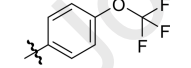
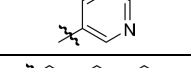
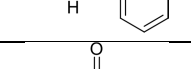
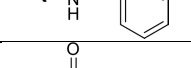
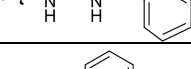
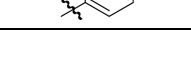
Cubist Pharmaceuticals designed a series of aryl-tetrazole IleRS inhibitors (Figure 1B), showing excellent selectivity with strong inhibition against pathogenic bacteria but not the eukaryotic enzyme. As compound **11k** exhibited most potent inhibition against *E. coli* LeuRS, we synthesized compound **15**, an analogue of the IleRS inhibitors while retaining the phenyl group connected with the heterocycle and substituting the isoleucyl with a leucyl moiety (Scheme 1C). Surprisingly, a

significant 15-fold reduction of activity was observed for **15** compared to **11k**. Two obvious distinctions between these two compounds can be noted: one is the six-membered pyran ring in **11k** versus the canonical five-membered anhydribose for **15**; the other one is the three-carbon linker between pyran and triazole in **11k** whereas a two-carbon linker was utilised for **15**. It is well known that mupirocin, an IleRS inhibitor, has a similar pyran ring in its chemical structure, and it has been reported that this pyran ring is recognized analogously to the ribose moiety of IleSA [5]. Therefore, it is reasonable to believe that the difference in activity between **11k** and **15** is attributed to the length of the carbon linker. This indicated a preference for a three-atom carbon linker for inhibitory activity possibly due to the shape or size of the binding site.

Overall, by analyzing their structure-activity relationship, it can be postulated that the precise length of the carbon linker and the chemical properties of the substituent on the triazole moiety are essential features for the inhibitory activity of this compound family targeting LeuRS.

Table 1. Inhibitory constants (K_i^{app}) of the synthesized compounds on *E. coli* LeuRS.



Compounds	R ^a	K_i^{app} (nM) ^d
11a		5.51 ± 0.93
11b		2969.71 ± 148.85
11c		52.36 ± 7.17
11d		108.35 ± 5.00
11e		387.66 ± 19.44
11f		17.83 ± 2.37
11g		31.62 ± 2.60
11h		1260.73 ± 92.11
11i		31.28 ± 2.37
11j		182.35 ± 4.20
11k		2.48 ± 0.13
15^b		30.94 ± 4.95
LeuSA^c		0.14 ± 0.10

^aR represents the various substituents connected to the triazole ring.

^b**15** is the analogue of a Cubist Pharmaceuticals IleRS inhibitor but carrying a leucyl moiety.

^cThe K_i^{app} value of high affinity inhibitor LeuSA was taken from our prior work [31].

^dA concentration of 2.5 nM *E. coli* LeuRS was used in the aminoacylation assay. The corresponding K_i^{app} values of the synthesized compounds were calculated using Greco-Hakala equation by maintaining the input enzyme concentration as a constant. All values were normalized based on the measured activity of the enzyme in the absence of inhibitor.

2.3. X-ray crystallographic studies of LeuRS-ligand bound complexes

To further elucidate the relative inhibitory activity and structural basis for the binding mechanism of this new series of LeuRS inhibitors, X-ray crystallographic studies of the compounds in complex with LeuRS were performed. *N. gonorrhoeae* LeuRS (Ng-LeuRS), a homologue to LeuRS from *E. coli* (Ec-LeuRS), was successfully crystallized and soaked with the compounds. We have previously reported that the overall sequence identity and similarity between these two enzymes is 57% and 71%, respectively, whereas the active site, which is responsible for the catalysis of Leu-AMP formation, share 92% identity and 100% similarity (Supplementary figure 2) [32]. Therefore, structural information obtained from Ng-LeuRS complexes can be extrapolated to the inhibition activity measured with *E. coli* LeuRS.

All Ng-LeuRS-ligand complexes were solved and determined at a resolution range between 1.9 and 2.6 Å (Supplementary table 1). Except for two low-affinity binders **11b** and **11h**, the remaining compounds can be built unambiguously in the catalytic site according to the electron density map (Figure 2). To gain further insight into the molecular mechanisms defining the inhibitory activity, we split the synthesized leucyl-sulfamoyl analogue scaffold into four pharmacophoric regions: leucyl-sulfamate moiety, the ring (six-member anhydrohexitol ring or 1,4-anhydroribitol for **15**), carbon linker (two-carbon or three-carbon linker for **15**) and various substitutions connected to either the triazole or tetrazole ring.

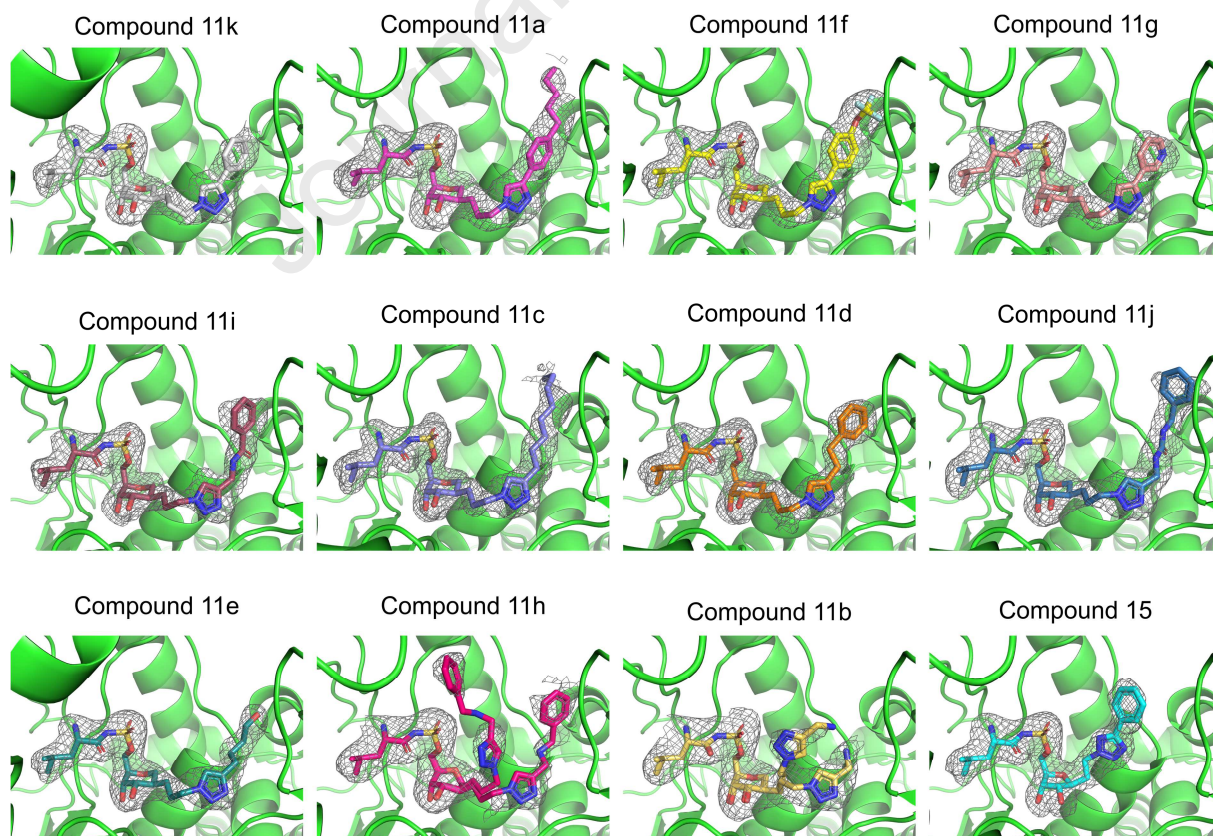


Figure 2. Omit maps of inhibitors bound to the active site of *N. gonorrhoeae* LeuRS. From left to right, structures are shown in order of decreasing inhibitory activity with the exception of compound **15**. The maps were calculated using phenix.polder and shown as a grey mesh framework contoured at 3.5σ . All ligands are shown as a stick representation where the catalytic site of LeuRS backbone is shown as a cartoon representation and colored in green. For compounds **11h** and **11b**, two different conformations are observed in the active site of enzyme due to weak binding.

Superposition of the structures of LeuRS in complex with **11a-k** by the catalytic core (mean RMSD of 0.22 Å with residues surrounding the ligand within 6 Å), shows that all compounds share very similar conformations (Figure 3A and Supplementary figure 3). The leucyl-sulfamate moiety is bound in the same pocket as observed for LeuSA (Figure 3B and 3D). Briefly, the amino group of the leucyl moiety forms H-bonds with O δ 2 of Asp80 and carbonyl oxygen in Phe41, while the carbonyl oxygen of the leucyl moiety itself forms a H-bond with N ϵ of His547. The side chain of the leucyl moiety is further recognized by a conserved hydrophobic pocket in all LeuRS structures, formed by Met40, Phe41, Tyr43, Phe507, Tyr513, His547 and His551 residues. The sulfamate oxygen further establishes either direct H-bonds with the main chain nitrogen of Tyr43 and N ϵ of His52 or *via* a water bridge with O ϵ 2 of Glu546 (Figure 3B). His52 is part of the class I signature HIGH motif, which in the case of Ng-LeuRS has the sequence ⁴⁹HMGH⁵². In further descriptions we will refer to any residues in this region using the former nomenclature. The tetrahydropyran adopts a chair conformation where the C1 atom is located in the same position as O4' of ribose and the 3-hydroxyl and 4-hydroxyl groups are superimposing with 2'- and 3'-hydroxyl of ribose in LeuSA, respectively. Therefore, the six-membered anhydrohexitol retains the same interactions as seen for ribose (Figure 3B). Compound **15** mimics the selective IleRS inhibitor CB 168 produced by Cubist Pharmaceuticals while replacing isoleucyl with a leucyl moiety. Comparing with LeuSA, the leucyl-sulfamoyl ribose moiety in **15** is fully superposed with the equivalent group in LeuSA and makes the same active site interactions observed for compounds **11a-k** and LeuSA (Figure 3C and 3D). Therefore, the obvious distinction in inhibitory activity of the synthesized compounds can be attributed to the linker and further substitutions on either the triazole or tetrazole ring.

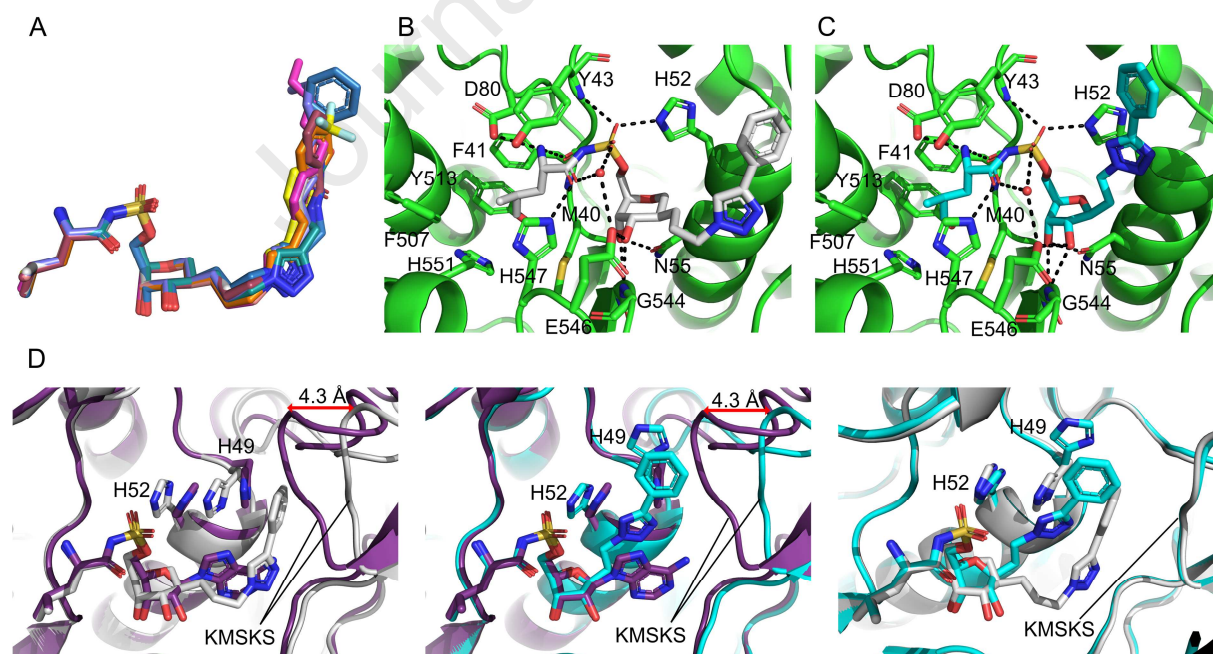


Figure 3. Comparison of compounds **11a-k** bound in *N. gonorrhoeae* LeuRS complexes. (A) Superposition of **11a-k** (except for **11b** and **11h**) by aligning the active site of the protein. (B) Interactions between leucyl-sulfamoyl anhydrohexitol moiety in **11k** and LeuRS. (C) Interactions between leucyl-sulfamoyl ribose moiety in **15** and LeuRS. Ligands and the interacting protein residues are shown as stick representations. The backbone of LeuRS is shown as a cartoon view. H-bonds are

shown as black dashed lines and water molecules as red spheres. (D) Left panel: Superposition of structures of **11k** and LeuSA (PDB code: 6Q89) [32]; Middle panel: Superposition of the structures **15** and LeuSA; Right panel: Superposition of the determined structures for **11k** and **15**. The movement of the KMSKS loop between the different structures was measured according to C α of the Lys637 residue.

In comparison with LeuSA, replacement of adenine with a propyl-triazole decorated with various phenyl modifications or aliphatic chains in the studied compounds, leads to disappearance of some extensive interactions as noted between the adenine ring and LeuRS protein residues, which explains the lower inhibitory activity observed for **11a-k** relative to LeuSA (Figure 4, 5 and Supplementary figure 4). In addition, to accommodate the binding of compounds **11a-k** and **15**, the KMSKS signature motif with the attached leucine specific domain (LSD) in LeuRS is positioned 4.3 Å outwards from the active site. Furthermore, the HIGH motif His49 rotates away from the active site compared to the LeuSA-bound structure (Figure 3D). This specific positioning of the KMSKS loop in these structural complexes establishes an enlarged open binding cavity for the synthesized inhibitors when compared to that seen when bound to LeuSA (Figure 3D and 4).

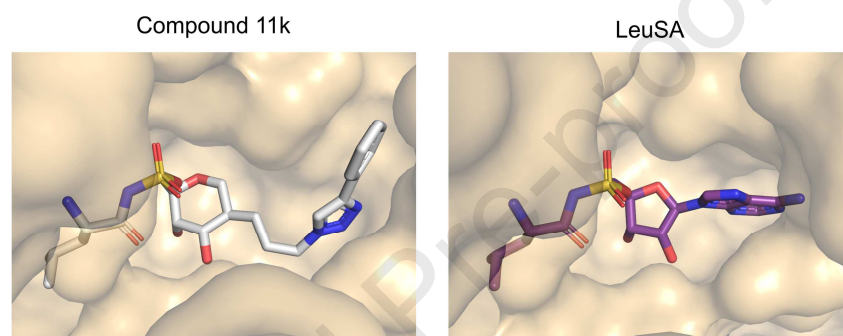


Figure 4. The binding pockets of compound **11k** and LeuSA in the respective LeuRS complexes. The protein is shown as surface representation and the ligands are shown as sticks.

To further investigate the forces defining the inhibitory activity, structural analysis of the interactions between the protein and the various substituents in compounds **11a-k** and **15** were performed (Figure 5). All compounds adopt a stretched conformation where the substituted triazole lies along the catalytic loop bearing the class I signature motif, ⁶³⁴KMSKS⁶³⁸, and stacking with the side chain of His49, being the first residue of the HIGH motif. As shown in Figure 5, the three-carbon atom linker apart from Van der Waals interactions does not make any specific interactions with the protein but provides the appropriate length to allow the triazole connecting group to move towards the binding cavity being positioned at the right side of adenine in the LeuSA complex structure. The N11 and N12 of the triazole heterocycle make one or two H-bonds with the backbone nitrogen of Val583. In addition, a cation- π interaction is formed with the side chain of Lys634 (Figure 5). For compounds **11k**, **11a**, **11f** and **11g**, an additional aromatic ring is directly connected to the triazole moiety, providing a supplementary π - π interaction with the imidazole of His49. Compounds **11a** and **11k** display the same interactions which further correlates with their comparable activities (Table 1). However, introduction of electron withdrawing substituents cause the aromatic ring to have weaker π - π interaction, which is the rationale for the decreased activities of compounds **11f** and **11g**.

In the remaining compounds various linkers connect the phenyl and triazole moieties. However, since the phenyl ring is moved away from His49, the contributing π - π interaction is lost, resulting in dramatically reduced binding affinity (Figure 5 and Table 1). However, compound **11i** demonstrated comparable activity to **11g**, which can be ascribed to the supplementary direct or indirect H-bond interactions between the carbonyl oxygen of the amide linker in **11i** and the backbone nitrogen of Met50 and carbonyl oxygen of Val643, respectively. In contrast, despite having similar H-bonds of the urea carbonyl oxygen for **11j**, the terminal phenyl ring becomes more exposed to the solvent resulting in increased entropic penalty and reduced binding capacity compared to **11i**. The aliphatic chain in compound **11c** and phenylethyl in **11d** are positioned parallel to the side chain of His49. Although losing the π - π interaction, their improved inhibitory activity compared to **11j** is likely the result of

hydrophobic interactions with the binding cavity. Moreover, introduction of a polar terminal hydroxyl group as in **11e** led to a 6-fold reduction in inhibitory activity versus **11c** (Table 1).

In view of the reduced length of the two-carbon atom linker in compound **15**, the binding mode for the tetrazole and phenyl rings is significantly different from that seen in compound **11k**. On superimposing with the LeuSA-bound structure, we noted the dihedral angle (O4'-C1'-C1-C2) in **15** is rotated 113.7° compared to the equivalent dihedral angle (O4'-C1'-N9-C8) in LeuSA. This results in the tetrazole and phenyl group being positioned further at left in the pocket than the adenine base (Figure 3D). The *Chi1* dihedral angle of His49 is simultaneously rotated 123.4° towards the opposite direction of the catalytic site to accommodate the binding of **15** and makes a π - π interaction between its phenyl ring and the His49 imidazole. Furthermore, the N4 nitrogen H-bonds with the backbone nitrogen of Gly51. Since compound **15** is rotated away from the binding cavity observed for compound **11k**, it only stacks with the HIGH motif and forms a weak cation- π contact with Lys634, but loses potential hydrophobic interactions resulting in its lower binding affinity compared to **11k**.

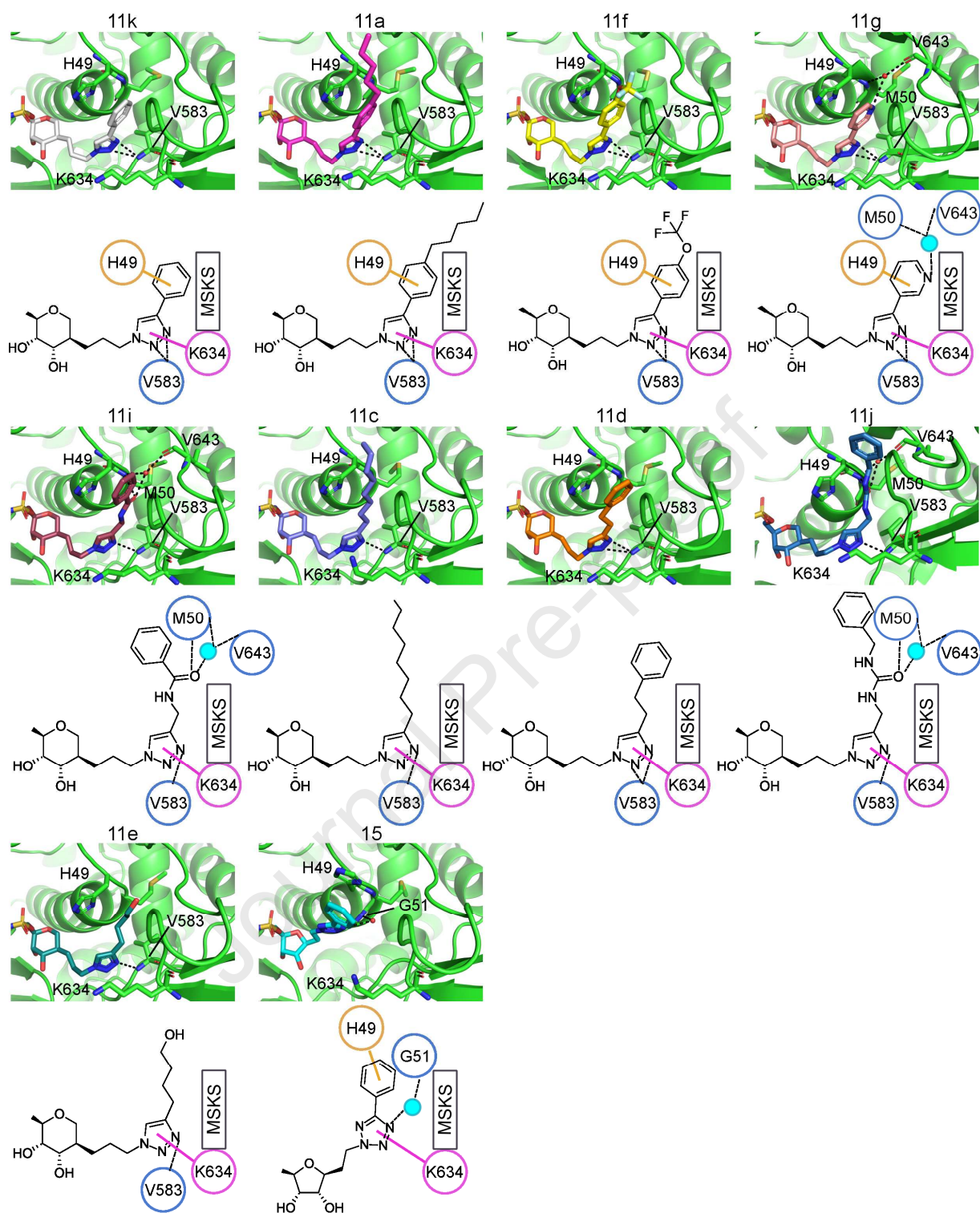


Figure 5. Analysis of protein-ligand interactions of the various inhibitor-bound *N. gonorrhoeae* LeuRS structures. Except for compound **15**, the remaining structures are shown in order of decreasing inhibitory activity. For each complex, 3D protein-ligand interactions are shown in the upper panel whereas the corresponding 2D interactions shown underneath. In the 3D interactions, protein structures are shown as cartoon representations while protein residues and ligands are shown as stick representations. All protein structures are colored in green. In 2D interactions, protein residues are shown as circles with numbers inside. KMSKS signature motif is shown as a black box with the starting residue in a magenta circle. Water molecules are shown as cyan filled circles. π - π stacking interaction is colored in orange, cation- π interaction is colored in magenta and all the remaining

interacting residues in blue. All H-bonds are shown as black dashed lines. The protein-ligand interactions are identified *via* the respective optimized structures in Schrödinger [36].

In the case of compounds **11b** and **11h**, electron density maps (Figure 2) clearly show the unambiguous binding of the leucyl-sulfamoyl anhydrohexitol moiety. However, two conformations for the aminomethyl-triazole part are observed for **11b**, while no clear density is detected for the substituent at the equivalent position in **11h**, demonstrating unstable binding of this part of the molecule for both compounds. Evaluating their chemical structure, it is worth noting that these two compounds are protonated at physiological pH, distinguishing them from the other studied inhibitors. To investigate the effect of a charged ligand, the relative electrostatic potential map was calculated for the LeuRS-**11b** complex. As shown in Figure 6, the protonated aminomethyl-triazole is located in a strongly positive charged cavity in LeuRS, leading to weak and flexible binding for this part of the molecule. In **11h** the benzylaminomethyl substituent on triazole is expected to lead to the same electronic repulsion, but the additional benzyl moiety apparently causes increased flexibility and hence lack of electron density is noted for this part of the molecule.

Taken together, the novel synthesized compounds demonstrated two distinct binding modes to their target LeuRS protein indicating a significant effect of the length of the linker. Further structural analysis for compounds **11a-k** showed that the various substituents on the triazole moiety either strongly contribute or reduce the inhibitory activity. Due to the positively charged binding pocket beyond the triazole ring, non-charged substituents are preferred over both positively charged examples. It can hence be postulated that a negative charged modification potentially could further enhance the binding affinity of an inhibitor. In particular IleRS, belonging to the same subclass as LeuRS, shares close homology and structural architecture in the active site region. The obtained data therefore can be employed to interpret the results of the early efforts of Cubist Pharmaceuticals in obtaining IleRS inhibitors and offer the possibility to design similar drugs binding to these enzymes.

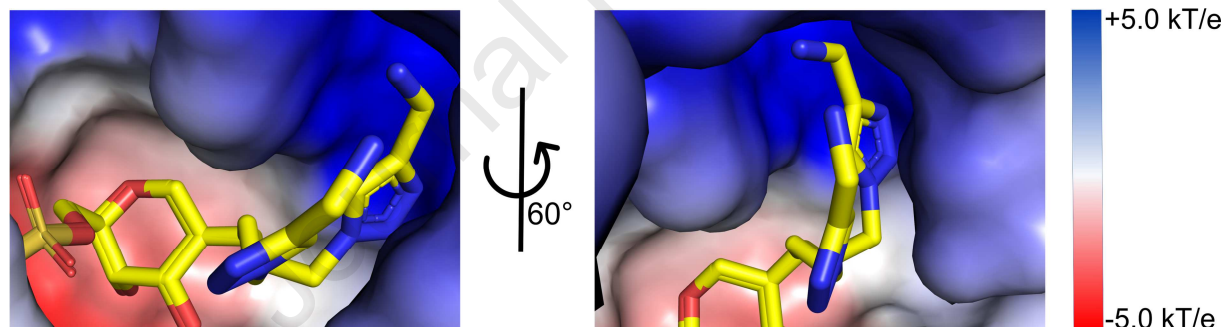


Figure 6. Electrostatic potential mapping on the protein surface surrounding ligand **11b**. The map was calculated using APBS Electrostatics in Pymol in which the blue, white and red represent the positively, neutral and negatively charged regions, respectively. Compound **11b** is shown as a stick representation and colored in yellow.

2.4. Antibacterial tests

Due to their potency against LeuRS, nine of the final synthesized 3-carbon atom linker compounds were screened for their *in vitro* antimicrobial activity against Gram-negative bacterium *Escherichia coli*, Gram-positive bacterium *Staphylococcus aureus* and yeast *Candida albicans*, using a previously established resazurin assay [37]. Although the lengths of LeuRSs from these different organisms vary considerably, comparison of the ligand binding site by sequence alignment clearly shows that all the important interacting residues are highly conserved in all tested species (Supplementary Figure 2). Only a small number of residues making backbone interactions are variable. Therefore, all these different LeuRSs should all be targeted by the synthesized LeuRS

inhibitors. Unfortunately, no antimicrobial activity was observed at the maximum concentration tested of 64 μM (data not shown).

These compounds were further evaluated for their *in vitro* activity against the Gram-positive non-pathogenic strain *Mycobacterium tuberculosis* (*Mtb*) H37Ra (ATCC® 25177TM) using a REMA assay (Table 2) [37]. While no anti-mycobacterial activity was observed for most of the compounds, analogue **11a** exhibited 86% inhibition at 128 μM providing a very modest IC_{50} value of 24.7 μM . In contrast, the Cubist-like compound **15** exhibited a five-fold reduced antimycobacterial activity with an IC_{50} of approximately 128 μM , which agrees with its decreased enzymatic activity comparing with **11a**.

Table 2. *In vitro* anti-mycobacterial activity test. Moxifloxacin, a first-line anti-TB drug with $\text{IC}_{50} = 0.25 \pm 0.13 \mu\text{M}$, was used as a positive control.

Compounds	% Inhibition at 128 μM
11a	86.08
11b	9.44
11c	4.26
11d	38.21
11e	23.24
11f	27.81
11g	16.85
11h	12.06
11k	4.24
15	49.83

3. Discussion and conclusion

Aminoacyl-tRNA synthetases are validated targets for the development of antimicrobials [3,38]. However, to date only mupirocin, a competitive IleRS inhibitor, and tavaborole, an antifungal molecule targeting the editing site of LeuRS, are commercially available (Figure 1A). Cubist Pharmaceuticals previously envisioned synthesis of selective IleRS and LeuRS inhibitors (Figure 1B) based on the high-affinity aminoacyl-sulfamate adenosine (aaSA) bio-isosteres (Figure 1B) of the active site intermediate (aa-AMP) [24,25]. We recently embraced the aryl-tetrazole strategy by Cubist Pharmaceuticals in combination with the tetrahydropyran ring of mupirocin. We therefore functionalized the C2 position with phenyltriazoles/tetrazoles using different linkers, while having the aminoacyl-sulfamate moiety in the same 1,4-cis arrangement as in mupirocin. Despite obtaining strong enzymatic inhibition for the IleRS triazole inhibitors with a three-atom spacer, no antibacterial activity was noted, which was attributed to the polarity of these molecules [30].

We now synthesized a series of LeuRS targeting compounds, having a C3 linker connecting the anhydrohexitol and the triazole heterocycle, with the latter carrying various substituents of different

polarities (Figure 1C). We redirected our research focus on LeuRS because compounds sharing similar scaffolds always displayed higher binding affinity with the target enzyme versus the equivalent analogs targeting IleRS [31,32]. Following synthesis of eleven LeuRS-targeted analogues using click chemistry (Scheme 1), their inhibitory constants were determined in an *in vitro* aminoacylation assay using purified recombinant *E. coli* LeuRS (Table 1) [32]. In comparison with LeuSA, their inhibitory activities clearly drop but most of them still inhibit in the lower nanomolar range with **11k** as most potent compound. However, some exceptions including compounds **11b** and **11j** showed a dramatic decrease in their inhibitory profile. To obtain a molecular understanding of their binding modes and establish a SAR study of these congeners with diverse polarity substitutions, *N. gonorrhoeae* LeuRS was crystallized and the corresponding enzyme-inhibitor structures were determined providing insights into the specific protein-ligand interactions.

All the new compounds clearly bind the canonical aminoacylation catalytic site of LeuRS. Comparing with LeuSA, the leucyl-sulfamoyl and six-membered pyran ring are recognized in the same manner as the equivalent leucyl-sulfamoyl ribose. Therefore, notable differences affecting the potential inhibition activity are highly related to the protein residues surrounding the triazole substitutions and the positioning of these triazole substitutions relative to each other and the adenine base in LeuSA. As described in our previous work [32], the adenine base makes several H-bonds with surrounding residues with the KMSKS-containing loop in a closed conformation. However, the long aliphatic chains or aromatic rings coupled to triazole bind in an enlarged cavity with an open conformation for the KMSKS motif (Figures 3 and 4). The substituted triazole in the synthesized compounds is sitting along KMSKS loop and stacked with the side chain of His49 of the HIGH motif. This binding mode of the synthesized inhibitors is very reminiscent of mupirocin binding to IleRS. It has been reported that the KMSKS loop is highly dynamic and can move in and out to assist the substrates binding during catalysis [39,40]. Therefore, the open conformation of the KMSKS loop in these inhibitor-bound structures indicates that these compounds are likely binding in the apo state of the enzyme. The loss of H-bonds as observed for the adenine congener provides a good rationale for the relative lower activity for the triazole series.

Further comparing the different substitutions demonstrates that the aromatic ring directly connected with triazole is essential for π - π and cation- π interactions explaining the good activity as seen for **11a**, **11f**, **11g** and **11k**. The phenyl-functionalized triazole **11k** proved to be the best LeuRS inhibitor with a K_i^{app} of 2.48 nM, only one order of magnitude less active than the high-affinity LeuSA bioisoster of the natural enzyme intermediate. Electron withdrawing substituents on this phenyl moiety have a negative impact on the enzymatic activity as seen for inhibitors **11f** and **11g**. The influence of an additional aliphatic chain on the aromatic ring is rather insignificant as noted for **11a** compared with **11k**. Replacing the aromatic ring with an aliphatic chain as in **11c** replicates the binding mode of the former but loses stacking interaction leading to its 10-fold decreased activity, but still inhibiting LeuRS with a K_i^{app} of 52 nM. This hints to similar binding as seen for mupirocin where the fatty acid-mimicking chain runs into a hydrophobic pocket in the active site of IleRS [41]. The activity drops when a more polar group is attached to the aliphatic chain as in **11e**.

In contrast, adding various length and polarity of linkers between triazole and aromatic ring has significant negative contribution for the binding affinity showing a 50 to 600-fold reduction. This is likely caused by the loss of stacking interaction and the solvent repulsive effect due to the aromatic benzene ring becoming exposed to the solvent. One exception is observed for compound **11i**, which appears to be complemented by the additional H-bonds generated with surrounding residues. Surprisingly, compounds **11b** and **11h** showed three orders of magnitude decreased inhibitory activity comparing with the most potent compound **11k**, which can be explained by the positive charged amine present in both former compounds. Electrostatics calculations of the protein shows that the binding pocket of this series of compounds is also positively charged indicating electron repulsive effects for these two compounds upon binding. Indeed, their electron density maps clearly suggest dynamic behavior in the pocket (Figure 2). However, the aminomethyl-substituted triazole **11b** was deliberately chosen in the design phase due to a recent report in which broad-spectrum antibiotics were obtained upon functionalization with this moiety. The rationale was that the aminomethyl moiety would improve uptake into bacterial cells with the molecule obeying to the so-called eNTRY rules [42]. The

interesting finding in this work suggests that designing negatively charged modifications at the *para*-position of the benzene ring in compound **11a** or totally replacing benzene could probably lead to improved LeuRS inhibitors as seen with the presence of the terminal carboxylic acid moiety in mupirocin.

In an attempt to have a good comparison for our best analogue **11k**, with the Cubist Pharmaceuticals compounds, we generated **15** using the two-atom carbon linker and standard ribose instead of pyran. Surprisingly, its activity is 15-fold lower than **11k** suggesting that the two-atom carbon linker is likely the determinant of the poorer activity. The X-ray crystallographic structure of **15**-bound LeuRS supports this hypothesis. While positioning of the leucyl-sulfamoyl ribose group is comparable to the equivalent moiety in **11k** the phenyltetrazole entity does not occupy the same part of the pocket as seen for **11k** as the two-atom linker is too short to explore this cavity. This results in a very different conformation of the phenyltetrazole group (Figure 3D).

Although demonstrating excellent *in vitro* activity against bacterial LeuRS, no broad-spectrum antibacterial activity including Gram-positive and Gram-negative pathogens was observed for the synthesized compounds which is likely the result of poor uptake. Interestingly, further antimycobacterial tests showed that compound **11a** exhibits the best albeit still weak activity with an IC₅₀ value of 24.7 μ M which is better than the similar compound **11k** indicating the aliphatic chain attached at the *para*-position of the benzene ring is important for mycobacterial uptake. The observed 5-fold improved activity compared to Cubist-like compound **15** suggests that our LeuRS inhibitor scaffold is however suited for further optimization. A potential solution for facilitating permeation is to ensure active uptake by bacterial cells by conjugation of a peptidic uptake signal or siderophore moiety. Such modifications are based on examples found in Nature as documented for the Trojan horse compounds microcin C and its analogues [43] which make use of a peptidic uptake signal and albomycin which contains a siderophore group for facilitated uptake [44]. Such strategies however need to be tailored for the specific species targeted but can also be used for targeting of mycobacteria as highlighted in a recent review [45].

In conclusion, we have uncovered inhibitor **11a** as a good starting compound for further optimization using the above proposed prodrug strategies in order to obtain antibacterial active molecules targeting LeuRS.

4. Experimental section

4.1. Reagents and analytical procedures

Reagents and solvents were purchased from commercial suppliers (Acros, Sigma-Aldrich) and used as provided, unless indicated otherwise. DMF, THF, DCM and MeOH were of analytical grade and were stored over 4 Å molecular sieves. All other solvents used for reactions were analytical grade and used as provided. Reactions were carried out in oven-dried glassware under a nitrogen atmosphere with stirring at room temperature, unless indicated otherwise. ¹⁴C-radiolabeled amino acids and scintillation liquid were purchased from Perkin Elmer. *E. coli* tRNA was purchased from Roche.

¹H and ¹³C NMR spectra of the compounds dissolved in CDCl₃, CD₃OD or DMSO-d₆ were recorded on a Bruker UltraShield Avance 300 MHz and 400 MHz or when needed on a 500 MHz and 600 MHz spectrometer. The chemical shifts are expressed as δ values in parts per million (ppm), using the residual solvent peaks (CDCl₃: ¹H, 7.26 ppm; ¹³C, 77.16 ppm; DMSO-d₆: ¹H, 2.50 ppm; ¹³C, 39.52 ppm; CD₃OD: ¹H, 3.31 ppm; ¹³C, 49.00 ppm) as a reference. Coupling constants are reported in Hertz (Hz). The peak patterns are indicated by the following abbreviations: br s = broad singlet, d = doublet, m = multiplet, q = quadruplet, s = singlet and t = triplet. High resolution mass spectra were recorded on a quadrupole time-of-flight mass spectrometer (SYNAPT G2 HDMS, Waters, Milford, US) equipped with a standard ESI interface; samples were infused in acetonitrile/H₂O (1:1) at 5 μ L/min. For TLC, precoated aluminum sheets were used (Merck, Silica gel 60 F254). The spots were visualized by UV light at 254 nm or when needed with 5% H₂SO₄ in EtOH. Chromatography was performed on ICN silica gel 60 Å 60-200. Eluent compositions are expressed as v/v. The

characterization of all intermediates and final compounds by NMR and mass spectrometry are provided in the supplementary file.

4.2. Chemical synthesis and analysis of intermediates and final compounds

4.2.1. (4*aR*,7*R*,8*S*,8*aS*)-7-allyl-2-phenylhexahydropyrano[3,2-*d*][1,3]dioxin-8-ol (2).

Copper(I) iodide (0.163 g, 0.85 mmol, 0.2 eq.) was put under an atmosphere of nitrogen and anhydrous tetrahydrofuran (THF, 15.7 mL) was added. The suspension was cooled to -30 °C and allylmagnesium chloride (10.7 mL, 5.0 eq., 2.0 M in THF) was added dropwise. Epoxide **1** (1.0 g, 4.27 mmol, 1.0 eq.) was dissolved in anhydrous THF (9.5 mL, 0.45 M) and was added dropwise to the Gilman-like reagent. The mixture was stirred for 1.5 h at -30 °C. After completion, the reaction was quenched with aqueous saturated ammonium chloride (50 mL) at -30 °C. The mixture was then stirred for 30 min. at room temperature. The aqueous layer was extracted with ethyl acetate (3x). The combined organic layers were washed with water and brine and dried over anhydrous MgSO₄. Following filtration, the solvent was removed under reduced pressure. The residue was purified by silica gel chromatography (heptane:ethyl acetate 50:50) to give compound **2** (0.810 g, 69%) with *R_f* = 0.70 (heptane:ethyl acetate 50:50) as a colourless oil. ¹H NMR (300 MHz, CDCl₃): δ = 7.53 – 7.44 (m, 2H), 7.42 – 7.31 (m, 3H), 5.77 (m, 1H), 5.62 (s, 1H), 5.11 (m, 2H), 4.30 (dd, *J* = 10.2, 4.8 Hz, 1H), 4.04 (s, 1H), 3.98 (dd, *J* = 11.7, 2.8 Hz, 1H), 3.94 – 3.85 (m, 1H), 3.76 – 3.67 (m, 2H), 3.64 (d, *J* = 11.6 Hz, 1H), 2.43 – 2.17 (m, 3H), 1.92 (dd, *J* = 8.7, 6.4 Hz, 1H) ppm. ¹³C NMR (75 MHz, CDCl₃): δ = 137.63, 136.31, 129.53, 128.64, 126.47, 117.42, 102.33, 77.95, 69.65, 68.73, 67.60, 66.11, 41.53, 34.48 ppm. HRMS (ESI): calcd. for C₁₆H₂₀O₄Na [M + Na]⁺ 299.1254; found 299.1253.

4.2.2. (4*aR*,7*R*,8*S*,8*aS*)-7-(3-hydroxypropyl)-2-phenylhexahydropyrano[3,2-*d*][1,3]dioxin-8-ol (3).

Alkene **2** (0.266 g, 0.96 mmol, 1.0 eq.) was put under an atmosphere of nitrogen and anhydrous THF (3.9 mL, 0.25 M) was added. Borane tetrahydrofuran complex (1.1 mL, 1.1 eq., 1.0 M in THF) was added and the mixture was stirred for 1 h at room temperature. After completion of the reaction, the solution was cooled to 0 °C. Aqueous sodium hydroxide (1.4 mL, 1.5 eq., 1.0 M) and aqueous hydrogen peroxide (0.1 mL, 1.5 eq., 35 wt.%) were added dropwise. The mixture was allowed to warm to room temperature and was stirred overnight at room temperature. The aqueous layer was extracted with ethyl acetate (3x). The combined organic layers were washed with aqueous saturated sodium bicarbonate and brine and dried over anhydrous MgSO₄. After filtration, the solvent was removed under reduced pressure. The residue was purified by silica gel chromatography (heptane:ethyl acetate 50:50 to 0:100) to afford compound **3** (0.258 g, 91%) with *R_f* = 0.12 (heptane:ethyl acetate 50:50) as a white solid. ¹H NMR (400 MHz, DMSO-*d*₆): δ = 7.45 (m, 2H), 7.35 (m, 3H), 5.64 (s, 1H), 4.98 (d, *J* = 3.5 Hz, 1H), 4.41 (t, *J* = 5.1 Hz, 1H), 4.13 (dd, *J* = 9.9, 4.8 Hz, 1H), 3.87 – 3.81 (m, 2H), 3.76 (td, *J* = 9.9, 4.9 Hz, 1H), 3.67 (dd, *J* = 9.4, 2.4 Hz, 1H), 3.62 (t, *J* = 10.1 Hz, 1H), 3.50 (d, *J* = 11.3 Hz, 1H), 3.41 (q, *J* = 5.7 Hz, 2H), 1.64 – 1.58 (m, 1H), 1.58 – 1.38 (m, 4H) ppm. ¹³C NMR (101 MHz, DMSO-*d*₆): δ = 138.49, 129.18, 128.38, 126.86, 101.47, 77.86, 68.96, 67.78, 67.15, 65.57, 61.16, 43.49, 31.30, 26.27 ppm. HRMS (ESI): calcd. for C₁₆H₂₂O₅Na [M + Na]⁺ 317.1360; found 317.1360.

4.2.3. (4*aR*,7*R*,8*S*,8*aS*)-7-(3-azidopropyl)-2-phenylhexahydropyrano[3,2-*d*][1,3]dioxin-8-ol (5).

Diol **3** (0.216 g, 0.73 mmol, 1.0 eq.) and triethylamine (0.2 mL, 1.1 mmol, 1.5 eq.) were put under nitrogen and anhydrous dichloromethane (DCM, 1.8 mL) was added. The solution was then cooled to -20 °C. *p*-Toluenesulfonyl chloride (TsCl; 0.140 g, 0.73 mmol, 1.0 eq.) was dissolved in anhydrous DCM (1.8 mL) and was added dropwise, resulting in a final 0.2 M solution. The mixture was allowed to warm to room temperature and was stirred overnight at room temperature. The reaction was quenched in cold water. The aqueous layer was extracted with DCM (3x). The combined organic layers were washed with water and brine and dried over anhydrous MgSO₄. After filtration, the solvent was removed under reduced pressure to yield crude compound **4**. HRMS (ESI): calcd. for C₂₃H₂₉O₇S [M + H]⁺ 449.1628; found 449.1628.

Sodium azide (0.072 g, 1.1 mmol, 1.5 eq.) was placed in a round bottom flask under nitrogen. Crude tosylate **4** was dissolved in anhydrous *N,N*-dimethylformamide (DMF, 3.7 mL, 0.2 M) and was added

to the sodium azide. The mixture was stirred overnight at 55 °C after which the solution was cooled to room temperature and water was added. The aqueous layer was extracted with ethyl acetate (3x). The combined organic layers were washed with water and brine and dried over anhydrous MgSO₄. After filtration, the solvent was removed under reduced pressure. The residue was purified by silica gel chromatography (heptane:ethyl acetate 50:50) to obtain compound **5** (0.218 g, 93%) with $R_f = 0.58$ (heptane:ethyl acetate 50:50) as a solid. ¹H NMR (400 MHz, CDCl₃): δ = 7.50 – 7.46 (m, 2H), 7.40 – 7.35 (m, 3H), 5.63 (s, 1H), 4.30 (dd, $J = 10.3, 5.0$ Hz, 1H), 4.02 (dd, $J = 11.7, 2.6$ Hz, 2H), 3.92 (td, $J = 10.1, 4.9$ Hz, 1H), 3.74 – 3.67 (m, 2H), 3.62 (d, $J = 11.7$ Hz, 1H), 3.39 – 3.27 (m, 2H), 2.35 (s, 1H), 1.86 – 1.80 (m, 1H), 1.78 – 1.50 (m, 4H) ppm. ¹³C NMR (101 MHz, CDCl₃): δ = 137.27, 129.26, 128.36, 126.14, 102.06, 77.72, 69.29, 68.85, 67.41, 65.90, 51.36, 41.47, 27.31, 26.78 ppm. HRMS (ESI): calcd. for C₁₆H₂₁N₃O₄Na [M + Na]⁺ 342.1424; found 342.1426.

4.2.4. ((3*aS*,4*R*,7*R*,7*aS*)-7-(3-azidopropyl)-2,2-dimethyltetrahydro-4*H*-[1,3]dioxolo[4,5-*c*]pyran-4-yl)methanol (**7**).

Azide **5** (1.1 g, 3.44 mmol, 1.0 eq.) and *p*-toluenesulfonic acid monohydrate (PTSA; 0.655 g, 3.44 mmol, 1.0 eq.) were put under an atmosphere of nitrogen and were dissolved in a 1:1 mixture of THF:water (23 mL : 23 mL, 0.075 M). The mixture was stirred for 3 days at 40 °C, after which the solvents were removed under reduced pressure to give crude compound **6** as a transparent oil. HRMS (ESI): calcd. for C₉H₁₇N₃O₄Na [M + Na]⁺ 254.1111; found 254.1111.

The obtained residue and an additional quantity of *p*-toluenesulfonic acid monohydrate (2.247 g, 11.8 mmol, 3.4 eq.) were dissolved in acetone (140 mL, 0.025 M). 2,2-Dimethoxypropane (DMP; 2.7 mL, 21.8 mmol, 6.3 eq.) was added and the mixture was stirred overnight at room temperature under nitrogen, after which the reaction was quenched with aqueous saturated sodium bicarbonate. Acetone was removed under reduced pressure and the remaining aqueous layer was extracted with ethyl acetate (3x). The combined organic layers were washed with water and brine and dried over anhydrous MgSO₄. Following filtration, the solvent was removed under reduced pressure and the residue was purified by silica gel chromatography (heptane:ethyl acetate 50:50) to afford compound **7** (0.866 g, 93%) with $R_f = 0.37$ (heptane:ethyl acetate 50:50) as a yellow oil. ¹H NMR (300 MHz, CDCl₃): δ = 4.11 (dd, $J = 4.9, 2.4$ Hz, 1H), 3.90 (dd, $J = 9.1, 5.1$ Hz, 1H), 3.86 – 3.75 (m, 2H), 3.67 (dd, $J = 11.7, 1.3$ Hz, 1H), 3.59 (m, 1H), 3.43 – 3.36 (m, 1H), 3.33 (m, 2H), 2.20 – 2.12 (m, 1H), 1.98 (m, 1H), 1.80 – 1.52 (m, 4H), 1.50 (s, 3H), 1.37 (s, 3H) ppm. ¹³C NMR (75 MHz, CDCl₃): δ = 109.26, 78.71, 76.29, 70.56, 65.96, 63.58, 51.63, 36.74, 28.47, 27.77, 27.13, 26.54 ppm. HRMS (ESI): calcd. for C₁₂H₂₁N₃O₄Na [M + Na]⁺ 294.1424; found 294.1423.

4.2.5. ((3*aS*,4*R*,7*R*,7*aS*)-7-(3-azidopropyl)-2,2-dimethyltetrahydro-4*H*-[1,3]dioxolo[4,5-*c*]pyran-4-yl)methyl sulfamate (**8**).

A flask was charged with nitrogen and was cooled to 0 °C. Chlorosulfonyl isocyanate (CSI; 0.9 mL, 10.7 mmol, 3.1 eq.) was added and then formic acid (0.4 mL, 10.8 mmol, 3.1 eq.) was added dropwise. The mixture was stirred for 30 min. at 0 °C. The resulting white solid was dissolved in anhydrous acetonitrile (10.7 mL, 1.0 M) and the solution was stirred for 5 h at room temperature. Alcohol **7** (0.935 g, 3.45 mmol, 1.0 eq.) was dissolved in *N,N*-dimethylacetamide (DMA; 17 mL) and was added dropwise to sulfamoyl chloride. The mixture was stirred overnight at room temperature, after which triethylamine (7.2 mL, 52 mmol, 15 eq.) was added and the mixture was stirred for 10 min. at room temperature. Methanol (MeOH, 7.0 mL, 172 mmol, 50 eq.) was then added, resulting in a transparent solution and the mixture was stirred for another 15 min. at room temperature. The solvents were removed under reduced pressure, and the residue was dissolved in aqueous saturated sodium bicarbonate. The aqueous layer was extracted with ethyl acetate (3x). The combined organic layers were washed with water and brine and dried over anhydrous MgSO₄. After filtration, the solvent was removed under reduced pressure and the residue was purified by silica gel chromatography (heptane:ethyl acetate 50:50) yielding compound **8** (0.964 g, 80%) with $R_f = 0.33$ (heptane:ethyl acetate 50:50) as a white oil. ¹H NMR (300 MHz, CDCl₃): δ = 5.14 (s, 2H), 4.39 (m, 1H), 4.30 – 4.19 (m, 1H), 4.18 – 4.11 (m, 1H), 3.89 (dd, $J = 9.3, 4.7$ Hz, 1H), 3.82 – 3.65 (m, 2H), 3.56 (dd, $J = 7.6, 5.9$ Hz, 1H), 3.32 (t, $J = 5.5$ Hz, 2H), 1.98 (m, 1H), 1.85 – 1.45 (m, 8H), 1.36 (s, 3H) ppm. ¹³C NMR (75

MHz, CDCl₃): δ = 109.71, 76.73, 76.12, 70.95, 69.79, 66.31, 51.58, 36.49, 28.48, 27.73, 27.11, 26.47 ppm. HRMS (ESI): calcd. for C₁₂H₂₃N₄O₆S [M + H]⁺ 351.1333; found 351.1338.

4.2.6. ((3*aS*,4*R*,7*R*,7*aS*)-7-(3-azidopropyl)-2,2-dimethyltetrahydro-4*H*-[1,3]dioxolo[4,5-*c*]pyran-4-yl)methyl ((tert-butoxycarbonyl)leucyl)sulfamate (**9**).

Cesium carbonate (2.69 g, 8.25 mmol, 3.0 eq.) was placed in a round bottom flask charged with nitrogen and was cooled to 0 °C. Compound **8** (0.964 g, 2.75 mmol, 1.0 eq.) and *t*-butyloxycarbonyl-*L*-leucine hydroxysuccinimide ester (1.807 g, 5.50 mmol, 2.0 eq.) were dissolved in anhydrous DMF (90 mL, 0.03 M) and were added. The mixture was gradually warmed to room temperature and was stirred for 3 days at room temperature. The solvent was then removed under reduced pressure and the residue was suspended in a 9:1 mixture of DCM:MeOH. The suspension was filtered over celite, and the solvent was removed under reduced pressure. The obtained residue was purified by silica gel chromatography (DCM:MeOH 95:5 to 90:10) to afford the leucine coupled compound **9** (1.551 g, 100%) with R_f = 0.07 (DCM:MeOH 90:10) as a yellow oil. ¹H NMR (300 MHz, CD₃OD): δ = 4.39 (dd, *J* = 10.8, 1.6 Hz, 1H), 4.29 – 4.16 (m, 2H), 4.10 (t, *J* = 7.4 Hz, 1H), 3.93 (dd, *J* = 9.0, 5.0 Hz, 1H), 3.70 (m, 2H), 3.63 – 3.53 (m, 1H), 3.37 (t, *J* = 6.5 Hz, 2H), 2.01 – 1.90 (m, 1H), 1.79 – 1.42 (m, 22H), 1.36 (s, 3H), 1.01 – 0.91 (m, 7H) ppm. ¹³C NMR (75 MHz, CD₃OD): δ = 108.53, 75.69, 75.57, 71.11, 69.18, 65.24, 50.75, 40.29, 35.21, 27.04, 26.84, 26.81, 26.08, 24.78, 24.23, 21.77, 20.19 ppm. HRMS (ESI): calcd. for C₂₃H₄₀N₅O₉S [M - H]⁻ 562.2552; found 562.2558.

4.2.7. ((3*aS*,4*R*,7*R*,7*aS*)-2,2-dimethyl-7-(3-(4-(4-pentylphenyl)-1*H*-1,2,3-triazol-1-yl)propyl)tetrahydro-4*H*-[1,3]dioxolo[4,5-*c*]pyran-4-yl)methyl ((tert-butoxycarbonyl)leucyl)sulfamate (**10a**).

Azide **9** (0.150 g, 0.27 mmol, 1.0 eq.), copper(I) iodide (0.005 g, 0.03 mmol, 0.1 eq.) and triethylamine (0.1 mL, 0.8 mmol, 3.0 eq.) were dissolved in DMF (1.3 mL, 0.2 M) and the solution was put under an atmosphere of nitrogen. 1-Ethynyl-4-pentylbenzene (0.1 mL, 0.53 mmol, 2.0 eq.) was added and the mixture was stirred overnight at 50 °C. The solvent was then removed under reduced pressure and the residue was purified by silica gel chromatography (DCM:MeOH 100:0 to 95:5) to give triazole **10a** (0.196 g, 100%) as a yellow oil. HRMS (ESI): calcd. for C₃₆H₂₆N₅O₉S [M - H]⁻ 734.3804; found 734.3838.

4.2.8. ((3*aS*,4*R*,7*R*,7*aS*)-7-(3-(4-(aminomethyl)-1*H*-1,2,3-triazol-1-yl)propyl)-2,2-dimethyltetrahydro-4*H*-[1,3]dioxolo[4,5-*c*]pyran-4-yl)methyl ((tert-butoxycarbonyl)leucyl)sulfamate (**10b**).

The same procedure as for **10a** was followed making use of 0.03 mL of propargylamine. Purification by silica gel chromatography was performed using DCM:MeOH 95:5 to 90:10 as the eluents affording triazole **10b** (0.082 g, 50%) with R_f = 0.24 (DCM:MeOH 90:10) as a yellow oil. HRMS (ESI): calcd. for C₂₆H₄₅N₆O₉S [M - H]⁻ 617.2974; found 617.2955.

4.2.9. ((3*aS*,4*R*,7*R*,7*aS*)-2,2-dimethyl-7-(3-(4-octyl-1*H*-1,2,3-triazol-1-yl)propyl)tetrahydro-4*H*-[1,3]dioxolo[4,5-*c*]pyran-4-yl)methyl ((tert-butoxycarbonyl)leucyl)sulfamate (**10c**).

The same procedure as for **10a** was followed making use of 0.1 mL of 1-decyne. Purification by silica gel chromatography was performed using DCM:MeOH 100:0 to 95:5 as the eluents giving triazole **10c** (0.187 g, 100%) with R_f = 0.35 (DCM:MeOH 90:10) as a yellow oil. HRMS (ESI): calcd. for C₃₃H₅₈N₅O₉S [M - H]⁻ 700.3960; found 700.3973.

4.2.10. ((3*aS*,4*R*,7*R*,7*aS*)-2,2-dimethyl-7-(3-(4-phenethyl-1*H*-1,2,3-triazol-1-yl)propyl)tetrahydro-4*H*-[1,3]dioxolo[4,5-*c*]pyran-4-yl)methyl ((tert-butoxycarbonyl)leucyl)sulfamate (**10d**).

The same procedure as for **10a** was followed making use of 0.08 mL of 3-butyn-1-ylbenzene. Purification by silica gel chromatography was performed using DCM:MeOH 100:0 to 95:5 as the eluents yielding triazole **10d** (0.185 g, 100%) with R_f = 0.43 (DCM:MeOH 90:10) as a yellow oil. HRMS (ESI): calcd. for C₃₃H₅₀N₅O₉S [M - H]⁻ 692.3334; found 692.3337.

4.2.11. ((3*aS*,4*R*,7*R*,7*aS*)-7-(3-(4-(4-hydroxybutyl)-1*H*-1,2,3-triazol-1-yl)propyl)-2,2-dimethyltetrahydro-4*H*-[1,3]dioxolo[4,5-*c*]pyran-4-yl)methyl ((tert-butoxycarbonyl)leucyl)sulfamate (**10e**).

The procedure as for **10a** was followed making use of 0.06 mL of 5-hexyn-1-ol. Purification by silica gel chromatography was performed using DCM:MeOH 100:0 to 90:10 as the eluents affording triazole **10e** (0.176 g, 100%) with $R_f = 0.18$ (DCM:MeOH 90:10) as a yellow oil. HRMS (ESI): calcd. for $C_{29}H_{50}N_5O_{10}S$ [M - H]⁻ 660.3284; found 660.3297.

4.2.12. ((3*aS*,4*R*,7*R*,7*aS*)-2,2-dimethyl-7-(3-(4-(4-(trifluoromethoxy)phenyl)-1*H*-1,2,3-triazol-1-yl)propyl)tetrahydro-4*H*-[1,3]dioxolo[4,5-*c*]pyran-4-yl)methyl ((tert-butoxycarbonyl)leucyl)sulfamate (**10f**).

The procedure as for **10a** was followed making use of 0.08 mL of 1-ethynyl-4-(trifluoromethoxy)benzene. Purification by silica gel chromatography was performed using DCM:MeOH 100:0 to 95:5 as the eluents giving triazole **10f** (0.200 g, 100%) with $R_f = 0.53$ (DCM:MeOH 90:10) as a yellow oil. HRMS (ESI): calcd. for $C_{32}H_{45}N_5O_{10}SF_3$ [M - H]⁻ 748.2844; found 748.2850.

4.2.13. ((3*aS*,4*R*,7*R*,7*aS*)-2,2-dimethyl-7-(3-(4-(pyridin-3-yl)-1*H*-1,2,3-triazol-1-yl)propyl)tetrahydro-4*H*-[1,3]dioxolo[4,5-*c*]pyran-4-yl)methyl ((tert-butoxycarbonyl)leucyl)sulfamate (**10g**).

The procedure as for **10a** was followed making use of 0.055 g of 3-ethynylpyridine. Purification by silica gel chromatography was performed using DCM:MeOH 100:0 to 95:5 as the eluents yielding triazole **10g** (0.139 g, 78%) with $R_f = 0.23$ (DCM:MeOH 90:10) as a yellow solid. HRMS (ESI): calcd. for $C_{30}H_{45}N_6O_9S$ [M - H]⁻ 665.2974; found 665.2994.

4.2.14. ((3*aS*,4*R*,7*R*,7*aS*)-7-(3-(4-((benzylamino)methyl)-1*H*-1,2,3-triazol-1-yl)propyl)-2,2-dimethyltetrahydro-4*H*-[1,3]dioxolo[4,5-*c*]pyran-4-yl)methyl ((tert-butoxycarbonyl)leucyl)sulfamate (**10h**).

The procedure as for **10a** was followed making use of 0.144 g of *N*-benzylprop-2-yn-1-amine (0.992 mmol, 3.7 eq.). Purification by silica gel chromatography was performed using DCM:MeOH 100:0 to 95:5 as the eluents affording triazole **10h** (0.189 g, 100%) with $R_f = 0.42$ (DCM:MeOH 90:10) as a brown oil. HRMS (ESI): calcd. for $C_{33}H_{51}N_6O_9S$ [M - H]⁻ 707.3443; found 707.3458.

4.2.15. ((3*aS*,4*R*,7*R*,7*aS*)-7-(3-(4-(benzamidomethyl)-1*H*-1,2,3-triazol-1-yl)propyl)-2,2-dimethyltetrahydro-4*H*-[1,3]dioxolo[4,5-*c*]pyran-4-yl)methyl ((tert-butoxycarbonyl)leucyl)sulfamate (**10i**).

The same procedure as for **10a** was followed making use of 0.085 g of *N*-(2-propyn-1-yl)benzamide. Purification by silica gel chromatography was performed using DCM:MeOH 100:0 to 95:5 as the eluents giving triazole **10i** (0.192 g, 100%) as a yellow oil. HRMS (ESI): calcd. for $C_{33}H_{49}N_6O_{10}S$ [M - H]⁻ 721.3236; found 721.3248.

4.2.16. ((3*aS*,4*R*,7*R*,7*aS*)-7-(3-(4-((3-benzylureido)methyl)-1*H*-1,2,3-triazol-1-yl)propyl)-2,2-dimethyltetrahydro-4*H*-[1,3]dioxolo[4,5-*c*]pyran-4-yl)methyl ((tert-butoxycarbonyl)leucyl)sulfamate (**10j**).

The same procedure as for **10a** was followed making use of 0.100 g of 1-benzyl-3-(prop-2-yn-1-yl)urea. Purification by silica gel chromatography was performed using DCM:MeOH 95:5 to 90:10 as the eluents yielding triazole **10j** (0.142 g, 71%) as a yellow oil. HRMS (ESI): calcd. for $C_{34}H_{52}N_7O_{10}S$ [M - H]⁻ 750.3502; found 750.3521.

4.2.17. ((3*aS*,4*R*,7*R*,7*aS*)-2,2-dimethyl-7-(3-(4-phenyl-1*H*-1,2,3-triazol-1-yl)propyl)tetrahydro-4*H*-[1,3]dioxolo[4,5-*c*]pyran-4-yl)methyl ((tert-butoxycarbonyl)leucyl)sulfamate (**10k**).

The same procedure as for **10a** was followed making use of 0.1 mL of phenylacetylene. Purification by silica gel chromatography was performed using DCM:MeOH 95:5 to 90:10 as the eluents affording

triazole **10k** (0.098 g, 55%) as a yellow solid. HRMS (ESI): calcd. for $C_{31}H_{46}N_5O_9S$ $[M - H]^-$ 664.3021; found 664.3011.

4.2.18. ((2*R*,3*S*,4*S*,5*R*)-3,4-dihydroxy-5-(3-(4-(4-pentylphenyl)-1*H*-1,2,3-triazol-1-yl)propyl)tetrahydro-2*H*-pyran-2-yl)methyl leucylsulfamate (**11a**).

Triazole **10a** (0.196 g, 0.27 mmol, 1.0 eq.) was placed under nitrogen and an 1:1 mixture of trifluoroacetic acid (TFA):water (0.5 mL:0.5 mL) was added. The mixture was stirred for 5 h at room temperature, after which more water was added and the reaction mixture was lyophilized. The residue was purified by silica gel chromatography (DCM:MeOH 95:5 to 90:10) to provide the desired final compound **11a** (0.159 g, 83%) with $R_f = 0.11$ (DCM:MeOH 90:10) as a white solid. 1H NMR (300 MHz, CD_3OD): $\delta = 8.32$ (s, 1H), 7.73 (d, $J = 8.1$ Hz, 2H), 7.24 (d, $J = 8.1$ Hz, 2H), 4.46 (t, $J = 6.9$ Hz, 2H), 4.37 (d, $J = 9.5$ Hz, 1H), 4.24 (dd, $J = 10.8, 5.5$ Hz, 1H), 3.93 – 3.84 (m, 2H), 3.83 – 3.70 (m, 2H), 3.62 (dd, $J = 9.9, 3.0$ Hz, 1H), 3.56 (d, $J = 11.4$ Hz, 1H), 2.62 (t, $J = 7.6$ Hz, 2H), 2.13 – 1.93 (m, 2H), 1.92 – 1.47 (m, 7H), 1.47 – 1.20 (m, 5H), 0.98 (t, $J = 6.0$ Hz, 6H), 0.90 (t, $J = 6.8$ Hz, 3H) ppm. ^{13}C NMR (75 MHz, CD_3OD): $\delta = 173.91, 147.26, 142.69, 128.28, 127.42, 125.00, 120.34, 74.44, 69.87, 69.33, 64.26, 64.03, 53.65, 49.65, 41.46, 40.06, 34.91, 30.84, 30.50, 27.69, 25.10, 23.87, 21.81, 21.50, 20.46, 12.66$ ppm. HRMS (ESI): calcd. for $C_{28}H_{44}N_5O_7S$ $[M - H]^-$ 594.2967; found 594.2972.

4.2.19. ((2*R*,3*S*,4*S*,5*R*)-5-(3-(4-(aminomethyl)-1*H*-1,2,3-triazol-1-yl)propyl)-3,4-dihydroxytetrahydro-2*H*-pyran-2-yl)methyl leucylsulfamate (**11b**).

In analogy, triazole **10b** (0.082 g, 0.13 mmol, 1.0 eq.) was deprotected and purified by silica gel chromatography using DCM:MeOH:triethylamine 90:10:0 to 80:20:0 to 70:30:1 as the eluents affording final compound **11b** (0.038 g, 60%) as a yellow solid. 1H NMR (300 MHz, D_2O): $\delta = 7.90 - 7.76$ (m, 1H), 4.34 (t, $J = 6.5$ Hz, 2H), 4.21 – 4.04 (m, 2H), 3.93 (m, 1H), 3.84 – 3.62 (m, 4H), 3.56 (m, 1H), 3.46 (m, 2H), 3.22 (s, 2H), 1.82 (m, 2H), 1.67 (m, 1H), 1.41 (m, 5H), 0.82 (t, $J = 5.2$ Hz, 6H) ppm. ^{13}C NMR (75 MHz, D_2O): $\delta = 123.57, 74.00, 69.76, 68.69, 64.33, 64.06, 54.55, 50.10, 41.69, 40.44, 34.90, 27.04, 24.72, 23.98, 21.88, 21.03$ ppm. HRMS (ESI): calcd. for $C_{18}H_{35}N_6O_7S$ $[M + H]^+$ 479.2282; found 479.2279.

4.2.20. ((2*R*,3*S*,4*S*,5*R*)-3,4-dihydroxy-5-(3-(4-octyl-1*H*-1,2,3-triazol-1-yl)propyl)tetrahydro-2*H*-pyran-2-yl)methyl leucylsulfamate (**11c**).

In analogy, triazole **10c** (0.187 g, 0.27 mmol, 1.0 eq.) was deprotected and purified by silica gel chromatography using DCM:MeOH 95:5 to 90:10 as the eluents yielding final compound **11c** (0.131 g, 88%) with $R_f = 0.07$ (DCM:MeOH 90:10) as a colourless solid. 1H NMR (300 MHz, CD_3OD): $\delta = 7.80$ (s, 1H), 4.39 (dd + t, 3H), 4.24 (dd, $J = 10.7, 5.3$ Hz, 1H), 3.95 – 3.83 (m, 2H), 3.82 – 3.70 (m, 2H), 3.65 – 3.49 (m, 2H), 2.70 (t, $J = 7.5$ Hz, 2H), 2.11 – 1.48 (m, 9H), 1.40 – 1.24 (m, 11H), 1.00 (t, $J = 6.0$ Hz, 6H), 0.90 (t, $J = 6.7$ Hz, 3H) ppm. ^{13}C NMR (75 MHz, CD_3OD): $\delta = 173.72, 147.57, 121.52, 74.44, 69.85, 69.33, 64.23, 64.00, 53.65, 49.45, 41.45, 40.07, 31.24, 28.84, 28.65, 28.57, 28.52, 27.67, 25.07, 24.58, 23.89, 21.93, 21.50, 20.47, 12.69$ ppm. HRMS (ESI): calcd. for $C_{25}H_{46}N_5O_7S$ $[M - H]^-$ 560.3123; found 560.3115.

4.2.21. ((2*R*,3*S*,4*S*,5*R*)-3,4-dihydroxy-5-(3-(4-phenethyl-1*H*-1,2,3-triazol-1-yl)propyl)tetrahydro-2*H*-pyran-2-yl)methyl leucylsulfamate (**11d**).

In analogy, triazole **10d** (0.185 g, 0.27 mmol, 1.0 eq.) was deprotected and purified by silica gel chromatography using DCM:MeOH 95:5 to 90:10 as the eluents resulting in final compound **11d** (0.122 g, 83%) with $R_f = 0.05$ (DCM:MeOH 90:10) as a colourless solid. 1H NMR (300 MHz, CD_3OD): $\delta = 7.65$ (s, 1H), 7.31 – 7.08 (m, 5H), 4.42 – 4.17 (m, 4H), 3.92 – 3.68 (m, 4H), 3.64 – 3.47 (m, 2H), 3.05 – 2.88 (m, 4H), 2.04 – 1.63 (m, 6H), 1.51 (m, 1H), 1.34 (m, 1H), 1.06 – 0.89 (m, 6H) ppm. ^{13}C NMR (75 MHz, CD_3OD): $\delta = 173.51, 146.63, 140.62, 127.81, 127.71, 125.46, 121.85, 74.42, 69.84, 69.45, 64.21, 63.97, 53.56, 49.41, 41.46, 40.05, 34.83, 27.64, 26.56, 24.97, 23.88, 21.52, 20.45$ ppm. HRMS (ESI): calcd. for $C_{25}H_{38}N_5O_7S$ $[M - H]^-$ 552.2497; found 552.2503.

4.2.22. ((2*R*,3*S*,4*S*,5*R*)-3,4-dihydroxy-5-(3-(4-(4-hydroxybutyl)-1*H*-1,2,3-triazol-1-yl)propyl)tetrahydro-2*H*-pyran-2-yl)methyl leucylsulfamate (**11e**).

In analogy, triazole **10e** (0.176 g, 0.27 mmol, 1.0 eq.) was deprotected and purified by silica gel chromatography using DCM:MeOH 90:10 to 80:20 as the eluents giving final compound **11e** (0.076 g, 55%) with $R_f = 0.04$ (DCM:MeOH 80:20) as a colourless solid. $^1\text{H NMR}$ (300 MHz, CD_3OD): $\delta = 7.82$ (s, 1H), 4.41 (t, $J = 6.9$ Hz, 2H), 4.32 (d, $J = 9.9$ Hz, 1H), 4.20 (dd, $J = 10.7, 5.4$ Hz, 1H), 3.88 (m, 2H), 3.76 (dd, $J = 9.1, 4.3$ Hz, 1H), 3.68 (dd, $J = 8.1, 5.0$ Hz, 1H), 3.58 (m, 4H), 2.74 (t, $J = 7.4$ Hz, 2H), 2.11 – 1.89 (m, 2H), 1.89 – 1.51 (m, 9H), 1.44 – 1.29 (m, 1H), 1.01 (t, $J = 6.1$ Hz, 6H) ppm. $^{13}\text{C NMR}$ (75 MHz, CD_3OD): $\delta = 174.27, 121.56, 74.51, 69.87, 68.83, 64.24, 63.98, 60.87, 53.83, 49.43, 41.46, 40.17, 31.31, 27.65, 25.14, 25.06, 24.33, 23.91, 21.45, 20.49$ ppm. HRMS (ESI): calcd. for $\text{C}_{21}\text{H}_{38}\text{N}_5\text{O}_8\text{S}$ [$\text{M} - \text{H}$] 520.2446; found 520.2448.

4.2.23. ((2*R*,3*S*,4*S*,5*R*)-3,4-dihydroxy-5-(3-(4-(4-(trifluoromethoxy)phenyl)-1*H*-1,2,3-triazol-1-yl)propyl)tetrahydro-2*H*-pyran-2-yl)methyl leucylsulfamate (**11f**).

In analogy, triazole **10f** (0.200 g, 0.27 mmol, 1.0 eq.) was deprotected and purified by silica gel chromatography using DCM:MeOH 95:5 to 90:10 as the eluents providing final compound **11f** (0.145 g, 89%) with $R_f = 0.05$ (DCM:MeOH 90:10) as a white solid. $^1\text{H NMR}$ (300 MHz, CD_3OD): $\delta = 8.45$ (s, 1H), 7.94 (d, $J = 8.8$ Hz, 2H), 7.34 (d, $J = 8.1$ Hz, 2H), 4.49 (t, $J = 6.9$ Hz, 2H), 4.37 (dd, $J = 10.7, 1.3$ Hz, 1H), 4.25 (dd, $J = 10.8, 5.5$ Hz, 1H), 3.94 – 3.84 (m, 2H), 3.83 – 3.71 (m, 2H), 3.66 – 3.53 (m, 2H), 2.16 – 1.93 (m, 2H), 1.88 – 1.74 (m, $J = 11.2, 6.3$ Hz, 3H), 1.74 – 1.55 (m, $J = 14.2, 13.7, 7.1$ Hz, 2H), 1.51 – 1.37 (m, $J = 13.5, 7.8$ Hz, 1H), 0.98 (t, $J = 5.9$ Hz, 6H) ppm. $^{13}\text{C NMR}$ (75 MHz, CD_3OD): $\delta = 173.79, 148.50, 145.79, 129.30, 126.66, 121.89, 121.10, 120.78, 118.50, 74.46, 69.87, 69.36, 64.28, 64.01, 53.66, 49.74, 41.47, 40.06, 27.65, 25.10, 23.87, 21.46, 20.45$ ppm. HRMS (ESI): calcd. for $\text{C}_{24}\text{H}_{33}\text{N}_5\text{O}_8\text{SF}_3$ [$\text{M} - \text{H}$] 608.2007; found 608.2017.

4.2.24. ((2*R*,3*S*,4*S*,5*R*)-3,4-dihydroxy-5-(3-(4-(pyridin-3-yl)-1*H*-1,2,3-triazol-1-yl)propyl)tetrahydro-2*H*-pyran-2-yl)methyl leucylsulfamate (**11g**).

In analogy, triazole **10g** (0.139 g, 0.21 mmol, 1.0 eq.) was deprotected and purified by silica gel chromatography using DCM:MeOH 90:10 to 80:20 as the eluents yielding final compound **11g** (0.089 g, 81%) as a colourless solid. $^1\text{H NMR}$ (300 MHz, CD_3OD): $\delta = 8.61$ (s, 1H), 8.37 (d, $J = 7.6$ Hz, 1H), 7.61 (s, 1H), 4.52 (t, $J = 6.6$ Hz, 2H), 4.34 (dd, $J = 10.4$ Hz, 1H), 4.21 (dd, $J = 10.1, 5.0$ Hz, 1H), 3.95 – 3.83 (m, 2H), 3.83 – 3.66 (m, 2H), 3.66 – 3.50 (m, 2H), 2.17 – 1.94 (m, 2H), 1.90 – 1.73 (m, 3H), 1.71 – 1.53 (m, 2H), 1.51 – 1.36 (m, 1H), 0.98 (t, $J = 6.0$ Hz, 6H) ppm. $^{13}\text{C NMR}$ (75 MHz, CD_3OD): $\delta = 174.44, 147.13, 145.01, 143.45, 133.93, 121.76, 74.53, 69.86, 68.89, 64.29, 63.98, 53.86, 49.84, 41.48, 40.17, 27.62, 25.08, 23.91, 21.46, 20.51$ ppm. HRMS (ESI): calcd. for $\text{C}_{22}\text{H}_{33}\text{N}_6\text{O}_7\text{S}$ [$\text{M} - \text{H}$] 525.2137; found 525.2139.

4.2.25. ((2*R*,3*S*,4*S*,5*R*)-5-(3-(4-((benzylamino)methyl)-1*H*-1,2,3-triazol-1-yl)propyl)-3,4-dihydroxytetrahydro-2*H*-pyran-2-yl)methyl leucylsulfamate (**11h**).

In analogy, triazole **10h** (0.189 g, 0.27 mmol, 1.0 eq.) was deprotected and purified by silica gel chromatography using DCM:MeOH 95:5 to 85:15 to 75:25 as the eluents affording final compound **11h** (0.076 g, 50%) with $R_f = 0.04$ (DCM:MeOH 90:10) as a yellow solid. $^1\text{H NMR}$ (300 MHz, CD_3OD): $\delta = 8.23$ (s, 1H), 7.62 – 7.26 (m, 6H), 4.56 – 4.23 (m, 8H), 3.86 (m, 2H), 3.68 (m, 2H), 3.62 – 3.47 (m, 2H), 2.08 – 1.93 (m, 2H), 1.89 – 1.59 (m, 4H), 1.51 – 1.31 (m, 2H), 1.05 – 0.94 (m, 6H) ppm. $^{13}\text{C NMR}$ (75 MHz, CD_3OD): $\delta = 174.43, 130.56, 129.58, 128.97, 128.56, 74.38, 69.64, 68.64, 63.82, 63.74, 53.67, 50.18, 49.87, 41.68, 40.72, 40.13, 27.29, 24.66, 23.91, 21.46, 20.42$ ppm. HRMS (ESI): calcd. for $\text{C}_{25}\text{H}_{39}\text{N}_6\text{O}_7\text{S}$ [$\text{M} - \text{H}$] 567.2606; found 567.2611.

4.2.26. ((2*R*,3*S*,4*S*,5*R*)-5-(3-(4-(benzamidomethyl)-1*H*-1,2,3-triazol-1-yl)propyl)-3,4-dihydroxytetrahydro-2*H*-pyran-2-yl)methyl leucylsulfamate (**11i**).

In analogy, triazole **10i** (0.192 g, 0.27 mmol, 1.0 eq.) was deprotected and purified by silica gel chromatography using DCM:MeOH 95:5 to 90:10 to 85:15 as the eluents giving final compound **11i**

(0.095 g, 61%) with $R_f = 0.01$ (DCM:MeOH 90:10) as a colourless solid. ^1H NMR (300 MHz, CD_3OD): $\delta = 8.99$ (s, 1H), 8.22 – 7.75 (m, 3H), 7.59 – 7.39 (m, 3H), 4.79 – 4.09 (m, 6H), 3.95 – 3.80 (m, 2H), 3.79 – 3.65 (m, 2H), 3.63 – 3.46 (m, 2H), 2.09 – 1.88 (m, 2H), 1.88 – 1.60 (m, 4H), 1.59 – 1.26 (m, 2H), 0.99 (t, $J = 5.6$ Hz, 6H) ppm. ^{13}C NMR (75 MHz, CD_3OD): $\delta = 174.15, 131.11, 127.87, 126.74, 74.43, 69.78, 69.04, 64.14, 63.96, 53.76, 49.67, 41.46, 40.12, 34.54, 27.56, 25.00, 23.89, 21.47, 20.45$ ppm. HRMS (ESI): calcd. for $\text{C}_{25}\text{H}_{37}\text{N}_6\text{O}_8\text{S}$ [$\text{M} - \text{H}$] $^-$ 581.2399; found 581.2404.

4.2.27. ((2*R*,3*S*,4*S*,5*R*)-5-(3-(4-((3-benzylureido)methyl)-1*H*-1,2,3-triazol-1-yl)propyl)-3,4-dihydroxytetrahydro-2*H*-pyran-2-yl)methyl leucylsulfamate (**11j**).

In analogy, triazole **10j** (0.142 g, 0.19 mmol, 1.0 eq.) was deprotected and purified by silica gel chromatography using DCM:MeOH 90:10 to 85:15 as the eluents providing final compound **11j** (0.095 g, 82%) with $R_f = 0.01$ (DCM:MeOH 90:10) as a colourless solid. ^1H NMR (300 MHz, CD_3OD): $\delta = 7.91$ (s, 1H), 7.42 – 7.14 (m, 5H), 4.52 – 4.16 (m, 8H), 3.93 – 3.80 (m, 2H), 3.80 – 3.65 (m, 2H), 3.64 – 3.46 (m, 2H), 2.08 – 1.85 (m, 2H), 1.73 (m, 4H), 1.58 – 1.43 (m, 1H), 1.35 (s, 1H), 0.99 (t, $J = 5.9$ Hz, 6H) ppm. ^{13}C NMR (75 MHz, CD_3OD): $\delta = 173.96, 139.56, 127.75, 126.51, 126.26, 74.37, 69.75, 69.11, 64.06, 63.97, 53.69, 49.66, 43.08, 41.52, 40.09, 34.83, 27.54, 24.99, 23.88, 21.49, 20.46$ ppm. HRMS (ESI): calcd. for $\text{C}_{26}\text{H}_{40}\text{N}_7\text{O}_8\text{S}$ [$\text{M} - \text{H}$] $^-$ 610.2664; found 610.2672.

4.2.28. ((2*R*,3*S*,4*S*,5*R*)-3,4-dihydroxy-5-(3-(4-phenyl-1*H*-1,2,3-triazol-1-yl)propyl)tetrahydro-2*H*-pyran-2-yl)methyl leucylsulfamate (**11k**).

In analogy, triazole **10k** (0.098 g, 0.15 mmol, 1.0 eq.) was deprotected and purified by silica gel chromatography using DCM:MeOH 90:10 to 85:15 as the eluents providing final compound **11k** (0.077 g, 100%) with $R_f = 0.10$ (DCM:MeOH 90:10) as a colourless solid. ^1H NMR (300 MHz, CD_3OD): $\delta = 8.38$ (s, 1H), 7.87 – 7.79 (m, 2H), 7.50 – 7.39 (m, 2H), 7.39 – 7.30 (m, 1H), 4.48 (t, $J = 7.1$ Hz, 2H), 4.34 (dd, $J = 10.9, 1.9$ Hz, 1H), 4.21 (dd, $J = 10.9, 5.5$ Hz, 1H), 3.93 – 3.85 (m, 2H), 3.82 – 3.74 (m, 1H), 3.70 – 3.53 (m, 3H), 3.37 (s, 1H), 2.13 – 1.93 (m, 2H), 1.88 – 1.74 (m, 3H), 1.70 – 1.54 (m, 2H), 1.50 – 1.38 (m, 1H), 1.29 (s, 1H), 0.99 (t, $J = 6.6$ Hz, 6H) ppm. ^{13}C NMR (75 MHz, CD_3OD): $\delta = 174.84, 147.18, 130.06, 128.23, 127.58, 125.00, 120.59, 74.54, 69.92, 68.88, 64.33, 64.00, 53.94, 49.66, 41.44, 40.28, 27.66, 25.13, 23.92, 21.43, 20.48$ ppm. HRMS (ESI): calcd. for $\text{C}_{23}\text{H}_{35}\text{N}_5\text{O}_7\text{S}$ [$\text{M} - \text{H}$] $^-$ 524.2184; found 524.2194.

4.2.29. *N*-benzylprop-2-yn-1-amine (**12**).

An oven-dried flask was put under an atmosphere of nitrogen and was loaded with benzaldehyde (0.2 mL, 2.4 mmol, 1.0 eq.), which was dissolved in anhydrous MeOH (9.4 mL, 0.25 M). Propargylamine (0.2 mL, 2.5 mmol, 1.1 eq.) and acetic acid (0.1 mL) were subsequently added and the reaction mixture was stirred overnight at room temperature. The solution was cooled to 0 °C and sodium borohydride (0.267 g, 7.1 mmol, 3.0 eq.) was carefully added in portions. The mixture was stirred for 2 h at room temperature, whereafter the reaction was quenched with aqueous sodium hydroxide (1.0 M) at 0 °C. The aqueous layer was extracted with ethyl acetate (3x). The combined organic layers were washed with water and brine and dried over anhydrous MgSO_4 . Following filtration, the solvent was removed under reduced pressure and the residue was purified by silica gel chromatography (heptane:ethyl acetate 25:75 to 0:100) yielding compound **12** (0.144 g, 42%) with $R_f = 0.66$ (ethyl acetate) as a yellow oil. ^1H NMR (300 MHz, CDCl_3): $\delta = 7.28$ (m, 8H), 3.86 – 3.76 (m, 2H), 3.38 (m, 2H), 2.24 (m, 1H), 1.80 (br s, 1H) ppm. ^{13}C NMR (75 MHz, CDCl_3): $\delta = 139.70, 128.77, 127.50, 82.38, 71.92, 52.58, 37.64$ ppm.

4.2.30. *N*-(prop-2-yn-1-yl)benzamide (**13**).

An oven-dried flask was put under an atmosphere of nitrogen and was loaded with benzoyl chloride (0.5 mL, 4.5 mmol, 1.25 eq.), which was dissolved in anhydrous DCM (10 mL). Triethylamine (1.0 mL, 7.3 mmol, 2.0 eq.) and propargylamine (0.2 mL, 3.6 mmol, 1.0 eq.), dissolved in anhydrous DCM (5.0 mL), were subsequently added, resulting in a final 0.25 M solution, and the reaction mixture was stirred overnight at room temperature. After completion, water was added and the aqueous layer was

extracted with DCM (3x). The combined organic layers were washed with water and brine and dried over anhydrous MgSO_4 . After filtration, the solvent was removed under reduced pressure and the residue was purified by silica gel chromatography (heptane:ethyl acetate 75:25 \rightarrow 50:50) resulting in compound **13** (0.553 g, 96%) with $R_f = 0.52$ (heptane:ethyl acetate 50:50) as a white solid. ^1H NMR (300 MHz, CDCl_3): $\delta = 7.87 - 7.70$ (m, 2H), 7.57 – 7.37 (m, 3H), 6.33 (s, 1H), 4.33 – 4.18 (m, 2H), 2.32 – 2.24 (m, 1H) ppm. ^{13}C NMR (75 MHz, CDCl_3): $\delta = 132.07, 128.93, 127.29, 72.19, 30.09$ ppm. HRMS (ESI): calcd. for $\text{C}_{10}\text{H}_{10}\text{NO}$ $[\text{M} + \text{H}]^+$ 160.0757; found 160.0752.

4.2.31. 1-benzyl-3-(prop-2-yn-1-yl)urea (**14**).

An oven-dried flask was put under an atmosphere of nitrogen and was loaded with benzyl isocyanate (0.2 mL, 1.6 mmol, 1.0 eq.), which was dissolved in anhydrous DCM (3.3 mL). Propargylamine (0.1 mL, 1.8 mmol, 1.1 eq.), dissolved in anhydrous DCM (3.3 mL), was added dropwise at 0 °C, resulting in a final 0.25 M solution, and the reaction mixture was stirred for 3 h at room temperature after slowly warming the solution to ambient temperature. A white solid **14** (0.305 g, 100%) was formed, which was filtered and dried under vacuum. ^1H NMR (300 MHz, $\text{DMSO}-d_6$): $\delta = 7.38 - 7.16$ (m, 5H), 6.49 (t, $J = 5.8$ Hz, 1H), 6.28 (t, $J = 5.6$ Hz, 1H), 4.21 (d, $J = 6.0$ Hz, 2H), 3.81 (dd, $J = 5.8, 2.4$ Hz, 2H), 3.07 (t, $J = 2.4$ Hz, 1H) ppm. ^{13}C NMR (75 MHz, $\text{DMSO}-d_6$): $\delta = 157.65, 140.80, 128.33, 127.17, 126.71, 82.64, 72.62, 43.12, 29.05$ ppm. HRMS (ESI): calcd. for $\text{C}_{11}\text{H}_{13}\text{N}_2\text{O}$ $[\text{M} + \text{H}]^+$ 189.1022; found 189.1023.

4.2.32. 2-deoxy-4,5-dihydroxy-1-[5-phenyltetrazole]-D-allo-heptitol-7-N-(leucyl)-sulfamate (**15**).

^1H NMR (300 MHz, CD_3OD): $\delta = 8.08-8.16$ (m, 2H), 7.48-7.57 (m, 3H), 4.81-4.88 (m, 2H), 4.11-4.24 (m, 3H), 3.99-4.07 (m, 1H), 3.77-3.89 (m, 2H), 3.60-3.68 (m, 1H), 2.36-2.53 (m, 1H), 2.18-2.32 (m, 1H), 1.74-1.87 (m, 2H), 1.58-1.69 (m, 1H), 0.96-1.03 (m, 6H) ppm. ^{13}C NMR (75 MHz, CD_3OD): $\delta = 129.75, 128.31, 126.98, 126.02, 81.79, 79.04, 74.27, 71.31, 68.13, 53.87, 49.61, 40.32, 32.38, 23.96, 21.42, 20.42$ ppm. HRMS (ESI): calcd. for $\text{C}_{20}\text{H}_{29}\text{N}_6\text{O}_7\text{S}$ $[\text{M}-\text{H}]^-$ 497.1824; found: 497.1815.

4.3. Cloning, expression and purification of *E. coli* and *N. gonorrhoeae* LeuRSs

Cloning, expression and purification of LeuRS from *E. coli* were performed as previously described [31]. The encoding sequence of *N. gonorrhoeae* LeuRS was amplified by a one-step PCR from the genomic DNA of bacterial strain *Neisseria gonorrhoeae* ATCC 49226. This reaction was carried out by using the high-fidelity Q5 DNA polymerase (New England Biolabs) with forward primer 5'-gcgaacagattggtggtggtATGCAAGAACATTACCAGCCCG-3' and reverse primer 5'-ttgttagcagaagcttaTTAGACGACGATGTTCCACCAGT-3', where the small letters represent the adaptor complementary to the plasmid, while the capital letters represent the annealing sequences and the underlined parts correspond to a glycine residue which was introduced before the start codon of LeuRS to facilitate the cleavage of the SUMO tag during purification. The PCR product was visualized and separated in agarose gel, followed by gel extraction and in-fusion cloning with linearized pETRUK vector containing a pI enhanced SUMO tag as described [31]. The assembled plasmid pETRUK-Ng-LeuRS was first propagated in *E. coli* NEB5 α and then confirmed by DNA sequencing (LGC genomics).

Ng-LeuRS construct was transformed into *E. coli* Rosetta (DE3) pLysS expression host. The selected colony was inoculated into 2 mL LB medium containing 100 $\mu\text{g}/\text{mL}$ ampicillin and 30 $\mu\text{g}/\text{mL}$ chloramphenicol and incubated at 37 °C with 250 rpm for 8 h. Then the pre-culture was transferred into 2 L ZYP-5052 auto-induction medium [46] supplemented with a final concentration of 1 mM ZnSO_4 (Sigma Aldrich) and 1 mL of antifoam SE-15 (Sigma Aldrich). The culture was grown overnight at 24 °C and when the $\text{OD}_{600\text{nm}}$ reached 4.0, temperature was decreased to 18 °C. After another 24 h of growth, cells were harvested by centrifugation at 4 °C and cell pellets were resuspended in cation exchange buffer A (CEXA) containing 25 mM HEPES pH 8, 200 mM NaCl, 5 mM β -mercaptoethanol (β -ME) and frozen in -80 °C.

For protein purification of Ng-LeuRS, cell pellet was thawed and further diluted using CEXA in a final 8:1 v/w (CEXA: weight of pellet) ratio supplemented with 100 U cryonase (Takara) and 10 mM

MgCl₂. Cells were lysed by sonication on ice and then clarified by centrifugation at 18,000 g at 4 °C for 30 min. The supernatant was loaded onto 5 mL Hitrap SP HP column (GE Healthcare Life Sciences). SUMO tag fused LeuRS protein bound onto the column and was eluted by applying a linear gradient 0-50% cation exchange buffer B (CEXB) comprising of 25 mM Hepes pH 8, 1000 mM NaCl, 5 mM β-ME. Corresponding protein fractions were collected and SUMO hydrolase was added in a 1:250 (m/m) ratio to remove SUMO tag. Due to the presence of additional glycine in front of the target protein LeuRS, the SUMO tag was more flexible and could be easily cleaved in 10 min on ice. The cleaved protein was dialyzed against 1 L buffer (20 mM Tris pH 7, 10% w/v glycerol and 5 mM β-ME) overnight at 4 °C and further dialyzed in the same fresh buffer for another 2 h to remove all salts. Then the protein was loaded onto HiTrap SP HP column to remove the SUMO tag and contaminants, followed by applying on anion exchange Hitrap Q HP column (GE Healthcare Life Sciences). After collecting the fractions from anion exchange chromatography, the protein was concentrated to 30 mg/mL using a concentrator (10 KDa, 50 mL, Millipore) by centrifugation at 4 °C, 4000 rpm and then flash frozen in liquid nitrogen and stored in -80 °C.

4.4. In vitro inhibitory activity determination with purified *E. coli* LeuRS

The inhibitory effects of synthesized compounds **11a-11k** and **15** were evaluated by a radiolabeled aminoacyl transfer assay as described in our prior work [31,32]. Briefly, 2.5 mM *E. coli* LeuRS in 20 mM Tris pH 7.5, 100 mM KCl, 10 mM MgCl₂, 5 mM β-ME and 5% (v/v) DMSO was preincubated with serial dilutions of different compounds at 37 °C for 10 min in the presence of 50 μM ¹⁴C-labeled leucine, 2 mg/mL *E. coli* total tRNA pool (Roche), and 0.25 mg/mL inorganic pyrophosphatase. A final concentration of 500 μM ATP was added to the mixture to start the reaction. After 4 min, the reaction was quenched by adding 4 μL buffer containing 0.2 M sodium acetate pH4, 0.1% (w/v) N-lauroylsarcosine and 5 mM unlabeled leucine. 20 μL aliquot was spotted on a 3MM Whatmann paper and precipitated utilizing 10% (w/v) cold trichloroacetic acid (TCA). All papers were washed twice with 10% (w/v) TCA and once with acetone at 10-minute intervals and dried in air. Each paper was transferred into a vial and soaked into 12 mL scintillation liquid. Subsequent measurements were performed by a scintillation counter. The apparent inhibition constants (K_i^{app}) of all LeuRS inhibitors were determined by applying Greco-Hakala equation [47].

4.5. Crystallization and X-ray data collection for *N. gonorrhoeae* LeuRS

The crystallization procedure of *N. gonorrhoeae* LeuRS was carried out using hanging drop vapor diffusion method as previously described [32]. A solution of 10 mg/mL Ng-LeuRS in crystallization buffer (10 mM Tris pH 7, 100 mM NaCl, 2.5 mM β-ME) was mixed with reservoir solution (20% w/v PEG 3350, 100 mM bis-tris propane pH 8.5 and 100 mM MgCl₂) and crystal seeds from earlier optimizations in a 0.75:1.0:0.25 (v/v/v) ratio. Suitable crystals were soaked with 2 mM of each compound prepared in an equivalent reservoir solution supplemented with 22% (v/v) ethylene glycol for 2 h. These crystals were subsequently mounted in cryo-loops and flash frozen in liquid nitrogen. Diffraction data were collected at 100 K at Synchrotron ESRF beamline Massif-3 (Grenoble, France) and Synchrotron Soleil beamline Proxima 1 and 2 (Paris, France).

4.6. Structure determination of *N. gonorrhoeae* LeuRS in complex with synthesized inhibitors

Collected datasets were processed using autoPROC processing pipeline [48]. The initial phase of Ng-LeuRS complexed with corresponding inhibitor was solved by molecular replacement in Phenix [49] using our published structure of Ng-LeuRS in complex with LeuSA (PDB code: 6Q89) as the start searching model by removing all the solvent and ligand LeuSA [32]. The resulting model was refined in Phenix.refinement and manually built in COOT [50]. All ligand restraints were generated by Grade Web Server (<http://grade.globalphasing.org>). The crystallographic data collection and corresponding refinement statistics are shown in Supplementary table 1. LeuRS-inhibitor interactions were analyzed in Schrödinger Maestro Software.

All the structures were deposited in PDB and the related accession codes are as follows: **6YKK, 6YKL, 6YKN, 6YKO, 6YKQ, 6YKS, 6YKT, 6YKU, 6YKV, 6YKW, 6YKX, 7A0P.**

4.7. Antimicrobial screening

Bacteria are cultured in MHB (Mueller Hinton Broth) and maintained on TSA (Tryptone Soy Agar). All cultures and assays are conducted at 37°C. *Mycobacterium tuberculosis* is cultured in 7H9 + 10% OADC. Compound stock solutions are prepared in 100% DMSO at 20 mM or mg/mL. The compounds are serially pre-diluted (2-fold or 4-fold) in DMSO followed by a further (intermediate) dilution in demineralized water to assure a final in-test DMSO concentration of <1%. Assays are performed in sterile 96-well microtiter plates, each well containing 10 µL of the watery compound dilutions together with 190 µL of bacteria inoculum (5×10^3 CFU/ml). Bacterial growth is compared to untreated-control wells (100% cell growth) and medium-control wells (0% cell growth). After 17 h incubation, bacterial viability is assessed fluorimetrically after addition of 20 µL resazurin per well. After 1/2 h at 37 °C, fluorescence is measured (λ_{ex} 550 nm, λ_{em} 590 nm). The results are expressed as % reduction in bacterial growth/viability compared to control wells and IC₅₀ (50% inhibitory concentration) is determined. *M. tuberculosis* H37Ra ATCC 2517, *S. aureus* ATCC6538 and *E. coli* ATCC8739 are used. The compounds are tested at 5 concentrations (64 - 16 - 4 - 1 and 0.25 µM or mg/ml). The compound is classified inactive when the IC₅₀ is higher than 15 µM (or µg/ml). Between 15 and 5 µM (or µg/ml), the compound is regarded as weakly active. Only when the IC₅₀ is lower than 5 µM (or µg/ml), the compound is classified as active and is evaluated further. Standard bacterial reference compounds include doxycyclin (IC₅₀ *S. aureus* 0.11 ± 0.06 µM; *E. coli* 0.73 ± 0.38 µM) and the first line anti-TB drug isoniazid (0.1 ± 0.07 µM) and moxifloxacin (0.25 ± 0.13 µM). The IC₅₀ is determined using an extended dose range (2-fold compound dilutions) still with a highest concentration of 128 µM. The IC₅₀ against *C. albicans* was determined by a 4-fold serial dilution of the test compounds in RPMI with a 1% DMSO background. The concentration used for the test compounds ranged from 64.0 µM to 3.9×10^{-3} µM. As a positive control substance, miconazole was selected at 0.25 µM.

4.8. Electrostatic surface potential calculation

Electrostatic surface potential of Ng-LeuRS was calculated using APBS electrostatic tool in Pymol. The protein molecule was prepared by adding hydrogens and missing side chain atoms, assigning partial charges and radii using the default setting in the program pdb2pqr. The linearized Poisson-Boltzmann equation was applied. Parameters of the calculation were: protein and water dielectric constants, 2 and 78, respectively; 150 mM ionic strength; size of the 3D grid, $257 \times 225 \times 225$. Finally, the result was displayed together with the protein structure, color-coded according to the electrostatic potential (± 5 kT/e). Negatively charged regions are presented in red, neutral regions in white and positively charged regions in blue.

4.9. Bioinformatic analysis of LeuRS protein sequences

Sequence alignment of *N. gonorrhoeae* LeuRS (Uniprot B4RNT1), *E. coli* LeuRS (Uniprot P07813), *S. aureus* LeuRS (Uniprot Q2FXH2), *M. tuberculosis* LeuRS (Uniprot P9WV1) and *C. albicans* cytosolic LeuRS (Uniprot A0A1D8PS12) and mitochondrial LeuRS2 (Uniprot A0A1D8PQ56) were performed in Jalview [51] by using Muscle web server.

Funding

This work was supported by the Research Fund Flanders [Fonds voor Wetenschappelijk Onderzoek, 1109117N to D.D.R., 12N5918N to D.C., G077814N to S.S. and A.V., G0A4616N to S.W. and A.V.]; the KU Leuven Research Fund [3M14022 to S.W. and A.V.]; and the Chinese Scholarship Council [to L.P.]. Mass spectrometry was made possible by the support of the Hercules Foundation of the Flemish Government [20100225-7].

Conflicts of interest

No conflicts of interest are declared.

Acknowledgement

The authors thank the Belgian FWO for providing a PhD Fellowship of the Research Foundation - Flanders to Dries De Ruyscher and a postdoctoral mandate to Davie Cappoen, and the China Scholarship Council for providing a scholarship to Luping Pang and KU Leuven and FWO-Flanders for financial support.

References

- [1] E.R. Fletcher, “No Time To Wait” – AMR Could Cause 10 Million Deaths Annually By 2050, Warns UN Report. <https://www.healthpolicy-watch.org/no-time-to-wait-amr-could-cause-10-million-deaths-annually-by-2050-warns-un-report/>, 2019 (accessed 18 November 2019).
- [2] World Health Organization, Global Action Plan on Antimicrobial Resistance. <https://www.who.int/antimicrobial-resistance/global-action-plan/en/>, 2015 (accessed 07 August 2020).
- [3] G.H.M. Vondenhoff, A. Van Aerschot, Aminoacyl-tRNA synthetase inhibitors as potential antibiotics. *Eur. J. Med. Chem.* 46 (2011) 5227-5236. <https://doi.org/10.1016/j.ejmech.2011.08.049>.
- [4] C.S. Francklyn, P. Mullen, Progress and Challenges in Aminoacyl-tRNA Synthetase-based Therapeutics. *J. Biol. Chem.* 294 (2019) 5365-5385. <https://doi.org/10.1074/jbc.REV118.002956>.
- [5] T. Nakama, O. Nureki, S. Yokoyama, Structural Basis for the Recognition of Isoleucyl-Adenylate and an Antibiotic, Mupirocin, by Isoleucyl-tRNA Synthetase. *J. Biol. Chem.* 276 (2001) 47387-47393. <https://doi.org/10.1074/jbc.M109089200>.
- [6] F.L. Rock, W. Mao, A. Yaremchuk, M. Tukalo, T. Crepin, H. Zhou, Y.K. Zhang, V. Hernandez, T. Akama, S.J. Baker, J.J. Plattner, L. Shapiro, S.A. Martinis, S.J. Benkovic, S. Cusack, M.R. Alley, An antifungal agent inhibits an aminoacyl-tRNA synthetase by trapping tRNA in the editing site. *Science* 316 (2007) 1759-1761. <https://doi.org/10.1126/science.1142189>.
- [7] G. Eriani, M. Delarue, O. Poch, J. Gangloff, D. Moras, Partition of tRNA synthetases into two classes based on mutually exclusive sets of sequence motifs. *Nature* 347 (1990) 203-206. <https://doi.org/10.1038/347203a0>.
- [8] N. Cveticic, J.J. Perona, I. Gruic-Sovulj, Kinetic Partitioning between Synthetic and Editing Pathways in Class I Aminoacyl-tRNA Synthetases Occurs at Both Pre-transfer and Post-transfer Hydrolytic Steps. *J. Biol. Chem.* 287 (2012) 25381-25394. <https://doi.org/10.1074/jbc.M112.372151>.
- [9] Y. Tang, D.A. Tirrell, Attenuation of the editing activity of the Escherichia coli leucyl-tRNA synthetase allows incorporation of novel amino acids into proteins in vivo. *Biochemistry* 41 (2002) 10635-10645. <https://doi.org/10.1021/bi026130x>.
- [10] J.F. Chen, N.N. Guo, T. Li, E.D. Wang, Y.L. Wang, CP1 domain in Escherichia coli leucyl-tRNA synthetase is crucial for its editing function. *Biochemistry* 39 (2000) 6726-6731. <https://doi.org/10.1021/bi000108r>.
- [11] H. Jakubowski, Quality control in tRNA charging. *Wiley Interdiscip Rev RNA* 3 (2012) 295-310. <https://doi.org/10.1002/wrna.122>.
- [12] S. Cusack, A. Yaremchuk, M. Tukalo, The 2 Å crystal structure of leucyl-tRNA synthetase and its complex with a leucyl-adenylate analogue. *EMBO J.* 19 (2000) 2351-2361. <https://doi.org/10.1093/emboj/19.10.2351>.
- [13] B.C. Das, P. Thapa, R. Karki, C. Schinke, S. Das, S. Kambhampati, S.K. Banerjee, P. Van Veldhuizen, A. Verma, L.M. Weiss, T. Evans, Boron chemicals in diagnosis and therapeutics. *Future Med. Chem.* 5 (2013) 653-676. <https://doi.org/10.4155/fmc.13.38>.
- [14] B.E. Elewski, R. Aly, S.L. Baldwin, R.F. Gonzalez Soto, P. Rich, M. Weisfeld, H. Wiltz, L.T. Zane, R. Pollak, Efficacy and safety of tavaborole topical solution, 5%, a novel boron-based antifungal agent, for the treatment of toenail onychomycosis: Results from 2 randomized phase-III studies. *J. Am. Acad. Dermatol.* 73 (2015) 62-69. <https://doi.org/10.1016/j.jaad.2015.04.010>.

- [15] P. Zhang, S. Ma, Recent development of leucyl-tRNA synthetase inhibitors as antimicrobial agents. *MedChemComm* 10 (2019) 1329-1341. <https://doi.org/10.1039/C9MD00139E>.
- [16] K. O'Dwyer, A.T. Spivak, K. Ingraham, S. Min, D.J. Holmes, C. Jakielaszek, S. Rittenhouse, A.L. Kwan, G.P. Livi, G. Sathe, E. Thomas, S. Van Horn, L.A. Miller, M. Twynholm, J. Tomayko, M. Dalessandro, M. Caltabiano, N.E. Scangarella-Oman, J.R. Brown, Bacterial Resistance to Leucyl-tRNA Synthetase Inhibitor GSK2251052 Develops during Treatment of Complicated Urinary Tract Infections. *Bacterial Resistance to Leucyl-tRNA Synthetase Inhibitor GSK2251052 Develops during Treatment of Complicated Urinary Tract Infections*. *Antimicrob. Agents Chemother.* 59 (2015) 289-298. <https://doi.org/10.1128/AAC.03774-14>.
- [17] J.B. Patel, R.J. Gorwitz, J.A. Jernigan, Mupirocin resistance. *Clin. Infect. Dis.* 49 (2009) 935-941. <https://doi.org/10.1086/605495>.
- [18] M. Antonio, N. McFerran, M.J. Pallen, Mutations affecting the Rossman fold of isoleucyl-tRNA synthetase are correlated with low-level mupirocin resistance in *Staphylococcus aureus*. *Antimicrob. Agents Chemother.* 46 (2002) 438-442. <https://doi.org/10.1128/aac.46.2.438-442.2002>.
- [19] E.E. Udo, L.E. Jacob, B. Mathew, Genetic analysis of methicillin-resistant *Staphylococcus aureus* expressing high- and low-level mupirocin resistance. *J. Med. Microbiol.* 50 (2001) 909-915. <https://doi.org/10.1099/0022-1317-50-10-909>.
- [20] J.G. Hurdle, A.J. O'Neill, L. Mody, I. Chopra, S.F. Bradley, In vivo transfer of high-level mupirocin resistance from *Staphylococcus epidermidis* to methicillin-resistant *Staphylococcus aureus* associated with failure of mupirocin prophylaxis. *J. Antimicrob. Chemother.* 56 (2005) 1166-1168. <https://doi.org/10.1093/jac/dki387>.
- [21] D. Tenero, G. Derimanov, A. Carlton, J. Tonkyn, M. Davies, S. Cozens, S. Gresham, A. Gaudion, A. Puri, M. Muliaditan, J. Rullas-Trincado, A. Mendoza-Losana, A. Skingsley, D. Barros-Aguirre, First-Time-in-Human Study and Prediction of Early Bactericidal Activity for GSK3036656, a Potent Leucyl-tRNA Synthetase Inhibitor for Tuberculosis Treatment. *Antimicrob. Agents Chemother.* 63 (2019), e00240-19. <https://doi.org/10.1128/AAC.00240-19>.
- [22] L. Li, M.T. Boniecki, J.D. Jaffe, B.S. Imai, P.M. Yau, Z.A. Luthey-Schulten, S.A. Martinis, Naturally occurring aminoacyl-tRNA synthetases editing-domain mutations that cause mistranslation in *Mycoplasma* parasites. *Proc. Natl. Acad. Sci. U.S.A.* 108 (2011) 9378-9383. <https://doi.org/10.1073/pnas.1016460108>.
- [23] C. Shi, D. Tiwari, D.J. Wilson, C.L. Seiler, D. Schnappinger, C.C. Aldrich, Bisubstrate Inhibitors of Biotin Protein Ligase in *Mycobacterium tuberculosis* Resistant to Cyclonucleoside Formation. *ACS Med. Chem. Lett.* 4 (2013) 1213-1217. <https://doi.org/10.1021/ml400328a>.
- [24] X.Y. Yu, J.M. Hill, G.X. Yu, W.H. Wang, A.F. Kluge, P. Wendler, P. Gallant, Synthesis and structure-activity relationships of a series of novel thiazoles as inhibitors of aminoacyl-tRNA synthetases. *Bioorg. Med. Chem. Lett.* 9 (1999) 375-380. [https://doi.org/10.1016/S0960-894X\(98\)00738-0](https://doi.org/10.1016/S0960-894X(98)00738-0).
- [25] P. Schimmel, J. Tao, J. Hill, Aminoacyl tRNA synthetases as targets for new anti-infectives. *FASEB J.* 12 (1998) 1599-1609. <https://doi.org/10.1517/13543784.9.8.1767>.
- [26] M.H. Charlton, R. Aleksis, A. Saint-Leger, A. Gupta, E. Loza, L. Ribas de Pouplana, I. Kaula, D. Gustina, M. Madre, D. Lola, K. Jaudzems, G. Edmund, C.P. Randall, L. Kime, A.J. O'Neill, W. Goessens, A. Jirgensons, P.W. Finn, N-Leucinyl Benzenesulfonamides as Structurally Simplified Leucyl-tRNA Synthetase Inhibitors. *ACS Med. Chem. Lett.* 9 (2018) 84-88. <https://doi.org/10.1021/acsmchemlett.7b00374>.
- [27] M. Teng, M.T. Hilgers, M.L. Cunningham, A. Borchardt, J.B. Locke, S. Abraham, G. Haley, B.P. Kwan, C. Hall, G.W. Hough, K.J. Shaw, J. Finn, Identification of bacteria-selective threonyl-tRNA synthetase substrate inhibitors by structure-based design. *J. Med. Chem.* 56 (2013) 1748-1760. <https://doi.org/10.1021/jm301756m>.
- [28] F. Zhang, J. Du, Q. Wang, Q. Hu, J. Zhang, D. Ding, Y. Zhao, F. Yang, E. Wang, H. Zhou, Discovery of N-(4-sulfamoylphenyl)thioureas as *Trypanosoma brucei* leucyl-tRNA synthetase inhibitors. *Org. Biomol. Chem.* 11 (2013) 5310-5324. <https://doi.org/10.1039/c3ob40236c>.
- [29] W.X. Xin, Z.Z. Li, Q. Wang, J. Du, M.Y. Zhu, H.C. Zhou, Design and synthesis of alpha-phenoxy-N-sulfonylphenyl acetamides as *Trypanosoma brucei* leucyl-tRNA synthetase inhibitors. *Eur. J. Med. Chem.* 185 (2020) 111827. <https://doi.org/10.1016/j.ejmech.2019.111827>.

- [30] D. De Ruyscher, L. Pang, C. Mattelaer, M. Nautiyal, S. De Graef, J. Rozenski, S.V. Strelkov, E. Lescrinier, S.D. Weeks, A. Van Aerschot, Phenyltriazole functionalized sulfamate inhibitors targeting tyrosyl- or isoleucyl-tRNA synthetase. *Bioorg. Med. Chem.* 28 (2020) 115580. <https://doi.org/10.1016/j.bmc.2020.115580>.
- [31] B. Zhang, S. De Graef, M. Nautiyal, L. Pang, B. Gadakh, M. Froeyen, L. Van Mellaert, S.V. Strelkov, S.D. Weeks, A. Van Aerschot, Family-wide analysis of aminoacyl-sulfamoyl-3-deazaadenosine analogues as inhibitors of aminoacyl-tRNA synthetases. *Eur. J. Med. Chem.* 148 (2018) 384-396. <https://doi.org/10.1016/j.ejmech.2018.02.013>.
- [32] M. Nautiyal, S. De Graef, L. Pang, B. Gadakh, S.V. Strelkov, S.D. Weeks, A. Van Aerschot, Comparative analysis of pyrimidine substituted aminoacyl-sulfamoyl nucleosides as potential inhibitors targeting class I aminoacyl-tRNA synthetases. *Eur. J. Med. Chem.* 173 (2019) 154-166. <https://doi.org/10.1016/j.ejmech.2019.04.003>.
- [33] C. Brockway, P. Kocienski, C. Pant, Unusual stereochemistry in the copper-catalysed ring opening of a carbohydrate oxirane with vinylmagnesium bromide. *J. Chem. Soc., Perkin Trans. 1* (1984) 875-878. <https://doi.org/10.1039/P19840000875>.
- [34] G.H. Vondenhoff, B. Gadakh, K. Severinov, A. Van Aerschot, Microcin C and albomycin analogues with aryl-tetrazole substituents as nucleobase isosters are selective inhibitors of bacterial aminoacyl tRNA synthetases but lack efficient uptake. *ChemBioChem* 13 (2012) 1959-1969. <https://doi.org/10.1002/cbic.201200174>.
- [35] D. De Ruyscher, L. Pang, S. De Graef, M. Nautiyal, W.M. De Borggraeve, J. Rozenski, S.V. Strelkov, S.D. Weeks, A. Van Aerschot, Acylated sulfonamide adenosines as potent inhibitors of the adenylate-forming enzyme superfamily. *Eur. J. Med. Chem.* 174 (2019) 252-264. <https://doi.org/10.1016/j.ejmech.2019.04.045>.
- [36] Schrödinger, LLC, New York, NY, 2020.
- [37] D. Cappoen, E. Torfs, T. Meiresonne, P. Claes, E. Semina, F. Holvoet, M.B. de Macedo, F. Cools, T. Piller, A. Matheussen, K. Van Calster, G. Caljon, P. Delputte, L. Maes, O. Neyrolles, N. De Kimpe, S. Mangelinckx, P. Cos, The synthesis and in vitro biological evaluation of novel fluorinated tetrahydrobenzo[j]phenanthridine-7,12-diones against *Mycobacterium tuberculosis*. *Eur. J. Med. Chem.* 18 (2019) 629-650. <https://doi.org/10.1016/j.ejmech.2019.07.052>.
- [38] N.H. Kwon, P.L. Fox, S. Kim, Aminoacyl-tRNA synthetases as therapeutic targets. *Nat. Rev. Drug Discov.* 181 (2019) 111549. <https://doi.org/10.1038/s41573-019-0026-3>.
- [39] A. Palencia, T. Crépin, M.T. Vu, T.L. Lincecum Jr, S.A. Martinis, S. Cusack, Structural dynamics of the aminoacylation and proofreading functional cycle of bacterial leucyl-tRNA synthetase. *Nat. Struct. Mol. Biol.* 19 (2012) 677-684. <https://doi.org/10.1038/nsmb.2317>.
- [40] T. Kobayashi, T. Takimura, R. Sekine, K. Vincent, K. Kamata, K. Sakamoto, S. Nishimura, S. Yokoyama, Structural Snapshots of the KMSKS Loop Rearrangement for Amino Acid Activation by Bacterial Tyrosyl-tRNA Synthetase. *J. Mol. Biol.* 346 (2005) 105-117. <https://doi.org/10.1016/j.jmb.2004.11.034>.
- [41] C.M. Thomas, J. Hothersall, C.L. Willis, T.J. Simpson, Resistance to and synthesis of the antibiotic mupirocin. *Nat. Rev. Microbiol.* 8 (2010) 281-289. <https://doi.org/10.1038/nrmicro2278>.
- [42] Y. Abouelhassan, A.T. Garrison, H. Yang, A. Chávez-Riveros, G.M. Burch, R.W. Huigens, Recent Progress in Natural-Product-Inspired Programs Aimed To Address Antibiotic Resistance and Tolerance. *J. Med. Chem.* 62 (2019) 7618-7642. <https://doi.org/10.1021/acs.jmedchem.9b00370>.
- [43] M. Serebryakova, D. Tsibulskaya, O. Mokina, A. Kulikovskiy, M. Nautiyal, A. Van Aerschot, K. Severinov, S. Dubiley, A Trojan-Horse Peptide-Carboxymethyl-Cytidine Antibiotic from *Bacillus amyloliquefaciens*. *J. Am. Chem. Soc.* 138 (2016) 15690-15698. <https://doi.org/10.1021/jacs.6b09853>.
- [44] A. Pramanik, U.H. Stroehrer, J. Krejci, A.J. Standish, E. Bohn, J.C. Paton, I.B. Autenrieth, V. Braun, Albomycin is an effective antibiotic, as exemplified with *Yersinia enterocolitica* and *Streptococcus pneumoniae*. *Int. J. Med. Microbiol.* 297 (2007) 459-469. <https://doi.org/10.1016/j.ijmm.2007.03.002>.
- [45] K.H. Negash, J.K.S. Norris, J.T. Hodgkinson, Siderophore-Antibiotic Conjugate Design: New Drugs for Bad Bugs? *Molecules* 24 (2019) 3314. <https://doi.org/10.3390/molecules24183314>

- [46] F.W. Studier, Protein production by auto-induction in high density shaking cultures. *Protein Expr. Purif.* 41 (2005) 207-234. <https://doi.org/10.1016/j.pep.2005.01.016>.
- [47] R.A. Copeland, *Evaluation of Enzyme Inhibitors in Drug Discovery: A Guide for Medicinal Chemists and Pharmacologists*, 2nd Edition, Evaluation of Enzyme Inhibitors in Drug Discovery: a Guide for Medicinal Chemists and Pharmacologists, 2nd Edition, 2013, pp. 245-285.
- [48] C. Vonrhein, C. Flensburg, P. Keller, A. Sharff, O. Smart, W. Paciorek, T. Womack, G. Bricogne, Data processing and analysis with the autoPROC toolbox. *Acta Crystallogr. D Biol. Crystallogr.* 67 (2011) 293-302. <https://doi.org/10.1107/S0907444911007773>.

Journal Pre-proof

- [49] P.D. Adams, P.V. Afonine, G. Bunkóczy, V.B. Chen, I.W. Davis, N. Echols, J.J. Headd, L.W. Hung, G.J. Kapral, R.W. Grosse-Kunstleve, A.J. McCoy, N.W. Moriarty, R. Oeffner, R.J. Read, D.C. Richardson, J.S. Richardson, T.C. Terwilliger, P.H. Zwart, PHENIX: a comprehensive Python-based system for macromolecular structure solution. *Acta Crystallogr. D.* 66 (2010) 213-221. <https://doi.org/10.1107/S0907444909052925>.
- [50] P. Emsley, B. Lohkamp, W.G. Scott, K. Cowtan, Features and development of Coot. *Acta Crystallogr. D Biol. Crystallogr.* 66 (2010) 486-501. <https://doi.org/10.1107/S0907444910007493>.
- [51] A.M. Waterhouse, J.B. Procter, D.M.A. Martin, M. Clamp, G.J. Barton, Jalview Version 2-a multiple sequence alignment editor and analysis workbench. *Bioinformatics* 25 (2009) 1189-1191. <https://doi.org/10.1093/bioinformatics/btp033>.

Highlights

- Eleven anhydrohexitol analogues targeting leucyl-tRNA synthetase (LeuRS)
- Several inhibitors showed enzymatic inhibitory activity in low nanomolar range
- Crystal structures of all compounds in complex with LeuRS determined
- SAR study revealed crucial interactions for obtaining enzymatic inhibitory activity

Journal Pre-proof